Schweizerische Eidgenossenschaft
Confédération suisse
Confederazione Svizzera
Confederaziun svizra

Federal Department of the Environment, Transport,
Energy and Communications DETEC

**Swiss Federal Office of Energy SFOE**
Energy Research and Cleantech Division

**Final report dated** February 12 2024

---

# S-DSM

## Sustainable Demand Side Management for a low Carbon Footprint operation of Buildings

---

**Date:** February 12 2024

**Location:** Bern

**Publisher:**
Swiss Federal Office of Energy SFOE
Energy Research and Cleantech
CH-3003 Bern
www.bfe.admin.ch

**Co-financing:**
die werke versorgung wallisellen ag
Industriestrasse 13, 8304 Wallisellen
https://www.diewerke.ch/

**Subsidy recipients:**
Empa
Ueberlandstrasse 129-133, 8600 Dübendorf
https://www.empa.ch/

HEIG-VD
Avenue des Sports 20, 1401 Yverdon-les-Bains
https://heig-vd.ch/

**Authors:**
Hanmin Cai, Empa UESL, hanmin.cai@empa.ch
Philipp Heer, Empa UESL, philipp.heer@empa.ch
Matthias Brandes, Empa UESL, matthias.brandes@empa.ch
Julie Rousseau, Empa UESL, julie.rousseau@empa.ch
Didier Beloin-Saint-Pierre, Empa TSL, didier.beloinsaintpierre@empa.ch
Sébastien Desvaux, HES-SO, heig-vd, sebastien.lasvaux@heig-vd.ch
Mija Frossard, HES-SO, heig-vd, mija.frossard@heig-vd.ch

**SFOE project coordinators:**
BFE Bereichsleiter: Andreas Eckmanns, andreas.eckmanns@bfe.admin.ch
BFE Programmleitung Gebäude & Städte: Nadège Vetterli, nadege.vetterli@anex.ch

**SFOE contract number:** SI/502165-01

# Zusammenfassung

Dieses Projekt konzentriert sich auf die Entwicklung und praktische die Validierung eines Gebäudeautomatisierungssystems, das lokal elektrische Energie optimal nutzt, um auf den CO2-Fussabdruck (CF) des Schweizer Stromnetzes zu reagieren. Das System zielt darauf ab, Zeiten mit kohlenstoffintensivem Verbrauch zu vermeiden und damit den nachhaltigen Gebäudebetrieb zu fördern. Das Projekt nutzte Daten und Validierung von zwei Standorten: dem Gebäudekomplex "K3" in Wallisellen, der für Büro-/Gewerbezwecke genutzt wird, und dem NEST-Demonstrator der Empa in Dübendorf, der für Wohnzwecke genutzt wird. An beiden Standorten wurden Erweiterungen an der Gebäudeautomation implementiert, um die Praktikabilität der Entwicklungen zu demonstrieren. Die Effektivität der Entwicklungen wurde gemessen, indem Daten aus einem Referenzjahr mit einem Jahr verbesserter Betriebsführung und Simulationen verglichen wurden.

Mehrere Beiträge wurden geleistet. Zunächst wurden die Ergebnisse des BFE EcoDynBat[1]-Projekts weiterentwickelt, was eine Auflösung von 15 Minuten bei der CF-Vorhersage ermöglichte. Diese Weiterentwicklung ermöglicht eine Echtzeitvorhersage des Kohlenstoff-Fussabdruckprofils, was es wiederum ermöglicht, prädiktive Algorithmen für Betrieb lokaler Energiesysteme zu nutzen. Dennoch traten Herausforderungen bei der Zugänglichkeit von öffentlichen Datensätzen für die CO2-Berechnung und -Vorhersage auf, insbesondere hinsichtlich der ENTSO-E-Datenqualität.

Zweitens zeigten Vergleiche zwischen prädiktiven und regelbasierten Algorithmus in Simulationen und Experimenten gemischte Ergebnisse. Am NEST trugen sowohl Lastverschiebung als auch die Installation von PV-Anlagen gleichermassen zu einer 12%igen Reduzierung des durchschnittlichen CO2-Fussabdrucks bei. Interessanterweise führte ein zusätzlicher Batteriespeicher zu keiner weiteren Reduzierung. Simulationen an K3 deuteten auf eine 20%ige Reduzierung des CO2-Fussabdrucks hin, während Experimente eine Verringerung um 14% zeigten, was die Herausforderungen bei der Übertragung von Simulation auf reale Begebenheiten verdeutlichte. Eine zusätzliche Normalisierung zeigte eine geringere Reduzierung des durchschnittlichen CO2-Fussabdrucks. Mehrere dazu beitragende Faktoren werden im Bericht erläutert.

Drittens zeigte ein neuartiger datengetriebener Regelalgorithmus Skalierbarkeit und Leistungsverbesserungen in Bezug auf thermischen Komfort und Energieeffizienz, wodurch eine technische Hürde für den gross angelegten Einsatz von Demand Side Management (DSM) überwunden wurde. Erste Erkenntnisse über die nationale Verteilung der Flexibilität beim Heizen von Gebäuden, deren Aktivierung durch Rundsteuersignale (Tag-Nacht Signal von Verteilnetzbetreiber) ähnelt, bereiten den Boden für umfassende Energiemanagementstrategien.

In den nächsten Schritten wird der Schwerpunkt auf der Lösung von Problemen im Zusammenhang mit der Qualität und Vollständigkeit der ENTSO-E-Daten liegen, wobei ein besonderes Augenmerk darauf liegt, diese Bedenken den Interessengruppen zu verdeutlichen, um Verbesserungen anzustossen. Darüber hinaus besteht die Notwendigkeit, die Koordination zwischen den Projektpartnern zu verbessern und Pipelines zu standardisieren, um die Skalierbarkeit der implementierten Lösungen zu gewährleisten. Darüber hinaus ist es unerlässlich, Zuverlässigkeitsbewertungen in die Quantifizierung von Flexibilität und Kohlenstoff-Fussabdruck-Reduzierungen zu integrieren. Schliesslich wird weitere Forschung durchgeführt, um die Nachhaltigkeit der vorgeschlagenen Regelstrategien zu bewerten und damit verbundene Ressourcennutzung zu adressieren.

---

[1] https://www.aramis.admin.ch/Texte/?ProjectID=41804

# Résumé

Ce projet se concentre sur le développement et les tests pratiques d'un système d'automatisation de la consommation d'électricité de bâtiments afin de minimiser l'Empreinte Carbone (EC) liée à leur utilisation du mix électrique Suisse. Le système développé vise ainsi à éviter les périodes de consommation où l'EC est élevé, favorisant une opération plus environnementalement durable des bâtiments. Le projet a utilisé des données et des validations provenant de deux sites : le complexe commercial "K3" à Wallisellen et le démonstrateur résidentiel NEST à Dübendorf. Les deux sites ont mis en œuvre des extensions de l'exploitation des bâtiments pour démontrer la praticabilité des développements d'un système de contrôle de la consommation d'électricité. L'efficacité de ces mises en œuvre a été mesurée en comparant les données d'une année de référence avec une année d'exploitation améliorée et des simulations.

Plusieurs contributions ont été apportées dans notre projet. Tout d'abord, les méthodes du projet OFEN nommé EcoDynBat ont été développées pour obtenir une résolution de 15 minutes lors de la prédiction du signal EC lié au mix électrique. Cette amélioration permet une prévision en temps réel du profil de l'EC, ce qui permet aux algorithmes prédictifs d'optimiser les opérations des systèmes énergétiques locaux. Néanmoins, des défis sont survenus avec l'extraction de jeux de données publics pour le calcul et la prévision de l'EC, en particulier concernant la qualité des données ENTSO-E.

Deuxièmement, la comparaison entre les résultats des simulations et des tests expérimentaux a révélé des résultats mitigés pour le système de contrôle. Dans le bâtiment NEST, le décalage de charge et l'installation de panneaux solaires ont contribué de manière égale à une réduction de 12 % de l'EC moyenne. Cependant, le stockage supplémentaire de batteries n'a pas entraîné de réduction supplémentaire. Les simulations liées aux installations du bâtiment K3 ont indiqué une réduction potentielle de 20 % de l'EC, tandis que les tests expérimentaux ont montré une diminution de 14 %, mettant en évidence des défis pour atteindre les performances théoriques du système. D'ailleurs, une normalisation supplémentaire a révélé une performance inférieure dans la réduction de l'EC moyenne. Plusieurs facteurs contributifs sont discutés en détail dans le rapport.

Troisièmement, un nouvel algorithme de contrôle piloté par les données a démontré une évolutivité et des améliorations de performance en termes de confort thermique et d'efficacité énergétique, traitant ainsi une barrière technique au déploiement à grande échelle de la gestion de la demande en électricité. Des premières observations sur la flexibilité du chauffage des bâtiments à l'échelle nationale, dont l'activation rappelle le contrôle par déphasage, posent les bases de stratégies complètes de gestion de l'énergie.

Dans les prochaines étapes, les efforts se concentreront sur la résolution des problèmes liés à la qualité et à l'exhaustivité des données ENTSO-E nécessaires à la prédiction de l'EC de l'électricité, en mettant particulièrement l'accent sur la sensibilisation de ces préoccupations auprès des parties prenantes pour initier des améliorations. De plus, il est nécessaire d'améliorer la coordination entre les partenaires du projet et de standardiser les pipelines pour assurer la mise en place des solutions à grande échelle. En outre, il est essentiel d'intégrer des évaluations de fiabilité dans la quantification de la flexibilité et des réductions de l'EC. Enfin, des recherches supplémentaires seront menées pour évaluer la durabilité des stratégies de contrôle proposées, en tenant compte de l'augmentation associée de l'utilisation des ressources.

# Summary

This project focuses on the development and practical testing of a building automation system that optimally utilizes electricity responding to the carbon footprint (CF) of the Swiss grid electricity. The system aims to avoid carbon-intensive consumption times, thereby promoting sustainable building operations. The project leveraged data and validation from two sites: the "K3" building complex in Wallisellen, used for office/commercial purposes, and the NEST demonstrator in Dübendorf, used for residential purposes. Both sites implemented the building operation extensions to demonstrate the practicability of the developments. The effectiveness of these implementations was measured by comparing data from a benchmark year with a year of improved operation and simulation cases.

Several contributions have been made. First of all, the results from the SFOE EcoDynBat Project have been enhanced, allowing for a 15-minute resolution in CF prediction. This improvement enables real-time forecasting of carbon footprint profile, which further allows predictive algorithms to optimize local energy system operations. Nonetheless, challenges arose with the extraction of public datasets for GWP calculation and forecasting, particularly concerning the ENTSO-E data quality.

Secondly, comparison between predictive and rule-based controllers in simulation and experiments revealed mixing results. At NEST, both load shifting and PV installation contributed equally to a 12% reduction in the average carbon footprint. However, additional battery storage did not yield further reduction. Simulation at K3 indicated a 20% carbon footprint reduction, while experiments showed a 14% decrease, highlighting challenges in reconciling simulation and real-world results. An additional normalization revealed a lower performance in reducing the average carbon footprint. Multiple contributing factors are discussed in detail in the report.

Thirdly, a novel data-driven control algorithm showcased scalability and performance enhancements in thermal comfort and energy efficiency, addressing a technical barrier to large-scale DSM deployment. Preliminary insights into national distribution building space heating flexibility, whose activation resembles ripple control, set the stage for comprehensive energy management strategies.

In the next steps, efforts will focus on addressing issues related to the quality and completeness of ENTSO-E data, with a particular emphasis on highlighting these concerns to stakeholders to initiate enhancements. Additionally, there is a need to enhance coordination among project partners and standardize pipelines to ensure scalability of the implemented solutions. Furthermore, it is essential to integrate reliability assessments into the quantification of flexibility and carbon footprint reductions. Lastly, further research will be conducted to evaluate the sustainability of the proposed control strategies, addressing associated increase in resource usage.

# Main findings

Throughout the project, four main findings are summarized below.

1. **Carbon footprint forecasting capability:** The development of a carbon footprint profile forecast tool utilizing publicly available datasets represents a crucial step in enabling emission-aware demand-side management. However, challenges remain in steadily extracting public datasets for global warming potential calculation and forecasting. The unexpected issues on completeness and quality of the ENTSO-E data over a one-year runtime forecasting period are notable findings. Although the report proposes potential solutions to these challenges, they are not fully resolved within the scope of this project.
2. **Improvement in predictive control operation:** The experimental results indicate a lower footprint reduction than that in simulation-based analysis due to several factors, including inherent differences in performance assessment between simulation and experiments, forecasting and modeling inaccuracies, hardware's actuation limitations, complexities in maintainability. Particularly in the case study K3, challenges in stakeholder coordination, system understanding, and interfacing due to the lack of implementation documentation and manufacturer support are highlighted. The technical issues can be partially mitigated by further standardization and integrating control solutions more directly into on-site management systems, instead of retrofitting them.
3. **Data-driven approaches for scalability:** Developing a new data-driven control algorithm for demand-side management is crucial. The algorithm shows potential for scalability and transferability, making it a promising foundation for future large-scale DSM schemes. This approach's adaptability to various scenarios enhances its applicability in real-world deployment.
4. **National distribution of building space heating flexibility**: The report provides insights into the distribution of space heating flexibility across different building types, ages, and climatic regions on a national scale, using the concept of a flexibility envelope for quantification. The study provides the basis for future research to merge theoretical flexibility potential with practical implementation gaps. The flexibility of buildings that can be exploited by using a ripple control signal is shown. This comprehensive approach offers a more realistic estimation of exploitable flexibility at the system level, contributing to national energy management strategies.

# Contents

# Abbreviations

| | |
|---|---|
| ANN | Artificial Neural Network |
| LR | Linear Regression |
| CF | Carbon Footprint |
| CHP | Combined Heat and Power |
| COP | Coefficient Of Performance |
| ehub | Energy Hub |
| ENTSO-E | European Network of Transmission System Operators for Electricity |
| EV | Electric Vehicle |
| DHW | Domestic Hot Water |
| DSO | Distribution System Operator |
| DSM | Demand Side Management |
| GHG | Greenhouse Gas |
| GWP | Global Warming Potential |
| HP | Heat Pump |
| MAE | Mean Absolute Error |
| MAPE | Mean Absolute Percentage Error |
| ML | Machine Learning |
| MPC | Model Predictive Control |
| NMAE | Normalized Mean Absolute Error |
| NRMSE | Normalized Root Mean Square Error |
| RES | Renewable Energy Resources |
| RMSE | Root Mean Squared Error |
| SH | Space Heating |
| SOC | State Of Charge |
| WP | Work Package |

# 1 Introduction

## 1.1 Background information and current situation

The building sector and its energy use are currently responsible for a significant share of the worldwide greenhouse gas (GHG) emissions, which raises questions about the sustainability of our current living habits. This also applies in Switzerland since ~50% of our final energy demand is linked to the building stock, with an increasing electricity demand depending on a national mix that presents substantial variations in its carbon footprint (CF) during the year. Moreover, current energy control practices in buildings are based on relatively simple rules to satisfy current energy demands without predictive considerations for future demands. For instance, domestic hot water (DHW) storage is mainly charged at night, and heat pumps solely operate within normalized temperature levels. Therefore, traditional load profiles are not coordinated with energy production from low-carbon-intensity sources. This means that periods when Swiss electricity presents a low CF are not necessarily linked with higher energy uses in buildings. Additionally, the increasing share of energy output from distributed renewable energy resources (RES) challenges the existing operation paradigm of power systems, which has been designed to distribute electricity from large central power plants to a low-voltage network for most consumers.

Moving energy uses in buildings when the electricity presents a lower CF requires the availability of a CF signal for the consumed electricity and thus necessitates developments in dynamic CF assessment and forecasting (Beloin-Saint-Pierre et al., 2020; Lédée et al., 2023). Results of the SFOE EcoDynBat project[2] (BFE, 2020) have shown substantial variability in the hourly CF of the Swiss electricity mix, which means that old and new buildings could reduce their CFs significantly by shifting their electricity needs during specific periods of the day with demand-side management (DSM). This potential reduction can then be optimized with data-driven operationalization of energy flexibility.

Several approaches have been proposed to consider hourly historical CF profiles of electricity in different countries (e.g. (Roux et al., 2017), (Vuarnoz and Jusselme, 2018)) and they show the importance of considering such variations. The electricity map web service (Electricity map, 2024) is another interesting solution that provides historical and 24-hour forecasted hourly CF values for many countries at the cost of a monthly subscription. All these options provide interesting insights on how dynamic CF assessment can be carried out. However, they often use outdated environmental databases for the CF of energy sources, focus on marginal electricity CF instead of average electricity CF (considering average CO2 support comparison with the empirical average emissions), and sometimes lack clarity on how they calculate forecasted values for the coming day (e.g., electricity map services). Such aspects need to be better understood and further developed to increase our trust in using hourly CF values of the Swiss electricity mix to manage the timings of energy demands in buildings.

Additionally, to prepare power systems for challenges from large-scale integration of RES, exploiting the energetic flexibility of buildings may provide a cost-efficient solution. Traditionally, ripple control infrastructure is the industry standard for exploiting building energy flexibility by shifting the electrical consumption of heat pumps (HPs) and electric boilers with fixed schedules. However, it has limited functionality and may not exploit flexibility effectively. (Li et al., 2021) shows that building energy flexibility has been a central topic of much research on the possibilities of energy flexibility. Currently, there is no common definition of flexibility, and field studies are very limited due to the lack of research infrastructure and the complexity of proposed methodologies. Therefore, it is necessary to investigate real platforms and consider possible simplification for timely adoption in practice. A review of experimental predictive control studies in buildings and flexibility quantification and provision, has been collected and published in (Cai and Heer, 2021).

[2] https://www.aramis.admin.ch/Grunddaten/?ProjectID=41804

## 1.2 Purpose of the project

This project aims to develop and practically test a building automation system that controls according to the CF signal of the Swiss electricity grid mix to support a more sustainable operation of buildings. Two control concepts shall be compared. On the one hand, a concept aiming at distribution network operators (DSO); on the other hand, a concept to be implemented directly at prosumers, i.e., the building. The general development of the method is followed by a practical test in an operational building in Wallisellen (for office/commercial use) and in the NEST demonstrator that is situated in Dübendorf (for residential use). At both locations, the building operation is extended to demonstrate the practicability of the developments. Expected reductions of the building's CF will be evaluated by comparing measurements of energy use data from a benchmark year with simulations or real-world data of a year when operations are controlled in selected buildings.

The work begins with further developments of the dynamic CF assessment methodology by building on the results of the SFOE EcoDynBat project. The goal will be to use more recent CF values for the considered energy sources in the Swiss electricity mix while also providing the option to have a dynamic CF signal at the 15-minute scale for all historical ENTSO-E data since 2017. This highly detailed historical profile will then be used as an input to train and test different machine learning-based forecasting algorithms that will predict the 15-minute CF profile of the Swiss electricity mix for a period that goes up to 48 hours in the future. While simulation-based analysis only requires historical data to design an S-DSM controller, experiments necessitate a real-time forecast. As shown in Figure 1, the S-DSM controller takes into account the forecast and outputs decisions, which are considered as input to the infrastructure.

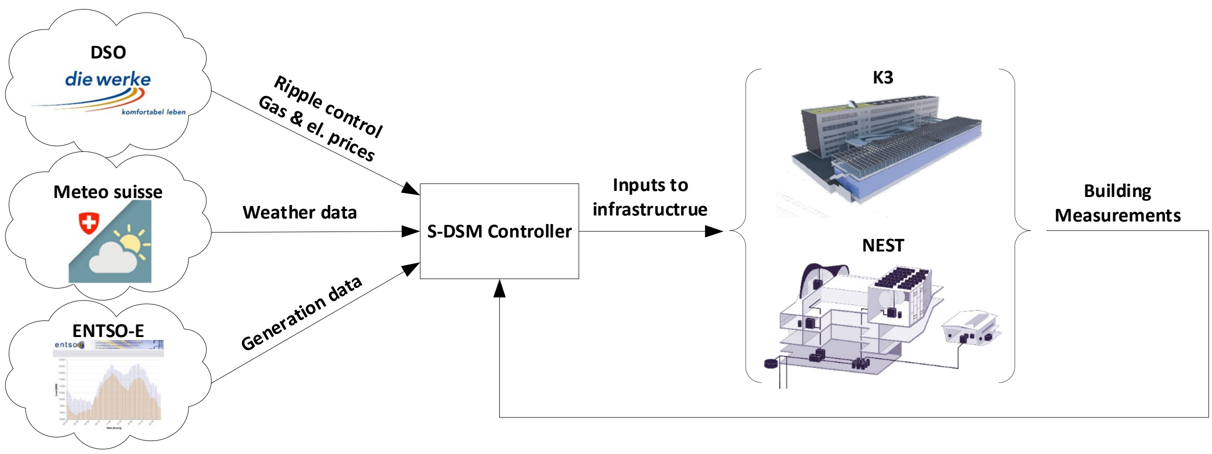


Figure 1. Project objective and illustration of overall closed-loop implementation of the controller including various exogenous inputs.

## 1.3 Objectives

The development of a forecasting algorithm for the average CF signal of the Swiss electricity mix, models of the energy infrastructure in buildings, and optimization-based controllers provide the basis to minimize buildings' equivalent direct and indirect GHG emissions due to electricity imported from the grid. The investigation into available flexibility and simplification options will offer practical tools to address challenges at a system level.

The results contained in this report contribute to addressing the following research questions:

1. How accurate can average CF forecasting be for the Swiss electricity mix, and what specific information is required for such a model?
2. How does predictive control operation compare to traditional rule-based controllers?

3. Which data-driven approach is best suited to enable scalable deployment of DSM?
4. How is building space heating demand flexibility, which can be exploited through the DSO approach, distributed nationally?

This report answers these questions with the following structure: Chapter 2 summarizes methodological development related to the research for the questions above. Chapter 3 outlines the quantitative results from simulation and experiments. Chapter 4 offers an overview of critical insights, while Chapter 5 suggests directions for future research.

# 2 Procedures and methodology

In this chapter, we first outline the initial project structure and procedures, followed by key methodological developments crucial to obtaining the results in Chapter 3. Sub-chapter 2.1 describes the overarching project plan and outlines the methodological interdependencies.

## 2.1 Project plan and connections with other projects

The S-DSM project utilizes knowledge from past and parallel projects. Namely, the SFOE EcoDynBat project and an Empa-funded project CAPITAL[3] feed WP1. In this WP, the EcoDynElec-Algorithm, derived from the SOFE EcoDynBat project, is developed further such that every 15 minutes, a CF-prediction is calculated with data fetched from several public and private sources. Hardware-oriented projects K3 supported by FOGA (Gasindustrie, 2024) and the continuing NEST project provide access to the respective measuring systems in WP2. The focus of this controllable data infrastructure lies on the energy hub components of K3 and NEST, which manage heating and cooling systems, as well as electrical storage. WP1 and WP2 feed their information into WP4, where the DSM strategies are developed. On the modeling side, the SFOE aliunid project (SFOE, 2020) and, again, CAPITAL reinforce the models of the buildings' energy infrastructure in WP3. These models serve as the development environment for the novel controller. They are also utilized in simulations to compare the current state of the industry controller with the S-DSM controller. The developments of WP1-WP4 are synthesized in WP5 and applied to the two implementation sites (K3 and NEST). The validation of the developments in operational conditions allows for an in-depth analysis of the developed method and shows the practical applicability of the approach. The collected measurement results in WP5 allow for a comparison between the developed S-DSM controller and the state of industry benchmark controller. A visual overview of the project's structure is shown in Figure 2.

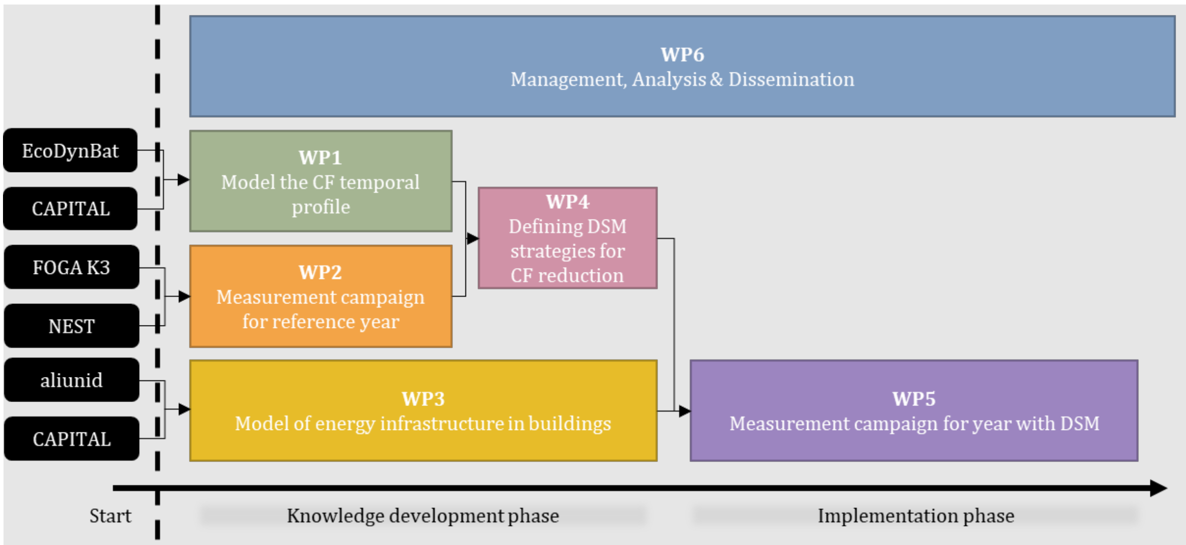


Figure 2. Project plan and synergies with other projects.

All WPs adopt data-driven approaches in that measured and/or collected real-time data is evaluated during runtime to make statements on the CF intensity of the Swiss electricity grid, inform the structure and parameters of simulation models, and determine which actions real-life systems should take over a multi-month period. Note that additional methodological developments and analyses have been carried out within this project's scope. Examples include developing data-driven control pipelines and

[3] https://www.empa.ch/web/s313/projects1 -> Chapter "CAPITAL"

analysis of flexibility potential from electric vehicles using onsite measurements. These works extend the methodological toolbox and provide an additional view of other flexibility resources.

The rest of this chapter details the overall methodology followed, with additional materials available in the Appendix for extended reference. Sub-chapter 2.2 corresponds with the HEIG-VD and Empa contributions and CAPITAL projects addressing research question 1, sub-chapter 2.3 incorporates elements from the aliunid and CAPITAL projects, while sub-chapter 2.4 merges aspects of the aliunid and CAPITAL projects. Both sub-chapter 2.3 and sub-chapter 2.4 contribute to answering research question 2. Sub-chapter 2.5 moves beyond the existing segmented control design workflow and tests novel data-driven control pipelines using the NEST infrastructure, answering research question 3. Sub-chapter 2.6 is formulated in collaboration with the CAPITAL project and leverages previously mentioned methods to analyze national flexibility distribution. Utilizing this identified flexibility potential bears a resemblance to the ripple control signal method. It is important to note that applying these methods is not necessarily sequential. Their interdependence is depicted in Figure 3.

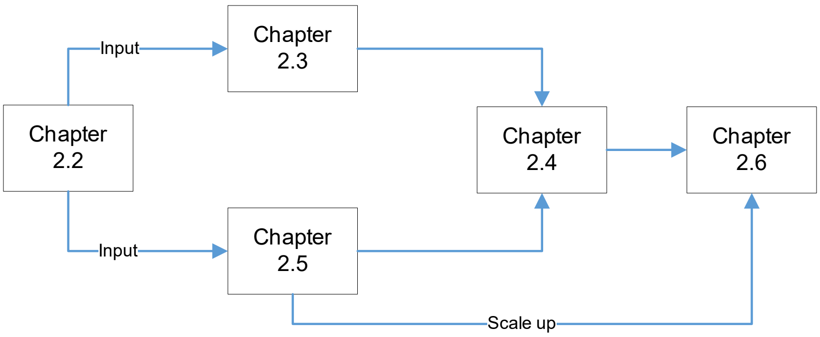


Figure 3. Overview of methodological developments and their dependencies.

## 2.2 Carbon footprint calculation and forecasting

The review of current existing CF forecasting methods for electricity mixes highlighted the existence of diverse options like the one from the work of the electricity map (Electricity map, 2024). Table 1 presents the key aspects of these identified methods.

Table 1. Overview of existing methods for “short-term” CF forecasting signals of electricity mixes.

| Reference | Year | Regions | Marginal or Average CF | Tested ML approaches | Selected ML approach | Data input for forecasting | Data for the GHG emissions of electricity sources | Range of forecast |
|---|---|---|---|---|---|---|---|---|
| Aryai | 2023 | Australia | Average | LSTM, ELM, ERT, DT, MLP | ERT and ELM | 1.5 year of data on electricity generation, demand and weather | Only GHG emissions from fuels and their combustion | 24-hour ahead |
| Bokde | 2021 | France, Germany, Norway, Denmark, Poland | Marginal | ARIMA, FFNN, PSF, DPSF | FFNN + ARIMA | ENTSO-E data for 2018-2019 - generation, demand, power | Country-specific CO2 emission intensity | 48-hour ahead |

| | | | | | | | | |
|---|---|---|---|---|---|---|---|---|
| Huber | 2021 | Germany | Marginal | MLP | MLP | ENTSO-E historic load and generation for 2017 + weather data | Direct CO2 emissions | 24-hour ahead |
| Leerbeck | 2020 | Denmark and neighboring regions | Average and Marginal | Several linear models + ARIMA | ARIMAX | See Tranberg 2019 and Electricity Map | From Electricity Map Service | 24-hour ahead |
| Maji | 2022 | US, Sweden, Germany | Average | CNN-LSTM | CNN-LSTM | Historical CF signal and weather forecast | US-EPA values for direct and CF | 96-hour ahead |
| Ostermann | 2024 | Germany | Average | SARIMAX, Bagging, Gradient Boosting, RF, CNN, LSTM, MLP | Gradient Bossting + RF | ENTSO-E production statistics between 2019-2022 (no imports/exports) | FfE platform for direct GHG emissions of sources | 24-hour ahead |
| Portolani | 2022 | Italy | Average | FNN, RNN, LR | FNN | ENTSO-E production data between 2016-2019 | Different impact categories (including GHG emissions) | 24-hour ahead |
| Riekstin | 2018 | USA, Canada, France | Average | LSTM (RNN variant) | LSTM | Historical data from past 28 days | GHG emission factors from ecoinvent v3.1 | 24-hour ahead |

We first found that the forecast signals in other articles are often made for marginal mixes instead of the average electricity mix that we want to use in the S-DSM project (e.g., Tranberg 2019, Leerbeck 2020a, Bodke 2021). Their analysis of the signal's volatility was thus less useful in our work to identify the most relevant criteria that could provide a good "short-term" forecast of the average CF for electricity (i.e., for 24 to 48 hours ahead). Most of these studies also stressed that the key input parameters and the performance of their ML approach depend on regional aspects. This was seen as an important knowledge gap for us since there have not been any studies for Switzerland. Our review of existing forecasting approaches also showed that they use various sources of information to describe the CF of the considered electricity sources and the training data (e.g., generation by source and weather data), and they select different ML approaches to make their forecasts. This remarkably diverse scope of choices for forecasting approaches currently hinders the identification of the most relevant and reliable strategy that might be followed.

This review of the state-of-the-art CF forecasting of electricity mixes prompted us to develop our own forecasting method based on the test of different ML approaches. An evaluation of the forecasting performance for the tested ML approaches was also made using the historical CF profile that was calculated with the EcoDynElec method (Lédée 2023). This analysis guided our choice for predicting the short-term future electricity production in Switzerland and enabled the runtime forecast needed for the other parts of the project.

### 2.2.1 Carbon footprint calculation for the Swiss electricity mix

The previous publications on the "short-term" forecasting of CF signals for the electricity mixes in different countries have shown that there are various methods to model the historical CF signal of electricity that consumers use. Many methods only consider domestic production(e.g., Huber 2021, Ostermann 2024), which gives a partial picture of the indirect GHG emissions and is inconsistent with the current electricity models in LCA studies.

The other common option relates to the work of Tranberg et al. 2019 that considers the exchanges between countries (i.e., with import and exports electricty flows) with a computational approach they call “flow tracing”. This model of the electricity network is similar to the current EcoDynElec model (Lédée 2023) and provides free of charge historical CF profiles of the electricity mix for Switzerland. However, in terms of short-term CF prediction, it only focuses on calculating marginal mixes.

Therefore, we can start our work for shortterm prevision of the CF profile with:

- either historical CF profiles of Electricity Maps
- or from EcoDynElec.

As consistency is key for our project and also becauase we need to calculate 15-minutes CF profile of the Swiss electricity mix, we rely on EcoDynElec datasets for which we have already calculated the data based on the previous SFOE EcoDynBat project.

The algorithms of the EcoDynBat method extract historical data from the ENTSO-E transparency platform (ENTSO-E, 2024) like many other methods (e.g., Electricity Map). The input data for the CF values of the considered energy sources comes from version 3.7.1 of the ecoinvent database (ecoinvent, 2020), which is a source that is rarely used by other methods even if it is recognized as one of the most reliable sources of LCA information in the world. This difference in the used CF for energy sources might be explained by the necessary subscription to access the ecoinvent database and its complexity which might be daunting for people who are not experts in environmental accounting.

The first development of the EcoDynBat method made in this project was to increase the level of temporal precision, going from an hourly description to a 15-minute scale. This was seen as an important development to enable change in electricity usage at a more rapid pace.

The newly developed algorithms could thus directly use the 15-minute data from the ENTSO-E transparency platform when it is available (e.g., for Austria and Germany). For countries that only provide hourly data (e.g., Czech Republic, France, Italy, and Switzerland), a disaggregation to 15-minute intervals was achieved through linear interpolation. This results in a limitation of representativeness for the 15-minute historical CF profile of the Swiss electricity mix but provides a signal that fits with the need of this project to consider rapid changes in electricity consumption. The new algorithms will work with more temporally precise information when such data becomes available for all countries.

A detailed description of the new algorithms can be found in (Lédée et al., 2023) and on a GitLab repository (https://github.com/LESBAT-HEIG-VD/EcoDynElec), which has become the reference place to find the latest version of the Python algorithms and share updates if they become necessary. These algorithms can provide a historical CF profile at the 15-minute scale while continuously getting the latest relevant statistics from the ENTSO-E platform. Additional detailed instructions on the calculation can also be found in the Appendix. These new algorithms, named the EcoDynElec method, were then used to create the input CF signal to train, test, and evaluate the different ML approaches that could forecast the “short-term” CF signal for the Swiss electricity mixes that are consumed in buildings.

The use of this new auto-updating CF calculation method showed that there are often issues with the quality/completeness of the ENTSO-E data (such as delayed reporting from power plants or invalid values) for the latest information (e.g., for the four most recent hours). Therefore, we limited the calculation of historical CF signals to data that was more than four hours old. The related 15-minute

CF profile in Switzerland (i.e., previous 28 days up to 4 hours before calculation) was then used as the input data for the forecasting of the short-term CF profile of the Swiss electricity mix. This limitation in the use of the latest information substantially influenced the runtime forecasting and consequently affected the potential for CF reduction, but resolving this issue is beyond our control.

### 2.2.2 Problem statements and offline training

An offline training using the combination of historical ENTSO-E data and CF of energy sources from ecoinvent (i.e., the dataset from EcoDynElec) was first carried out to evaluate if we could forecast the "short-term" CF signal with this information. The objective of this training was to forecast the 24-hour GHG profile $y$ for the following day $d+1$ using data available up to the end of day $d$.

In this training, the input dataset from the EcoDynElec method undergoes standardization wherever suitable using the MinMaxScaler to achieve uniform scaling of features, which is also applied to all test data. A grid search approach is employed for hyperparameter optimization. The model is trained and evaluated across a predefined grid of hyperparameter values. The optimal hyperparameters yield the best performance, as determined by 5-fold cross-validation with the negative mean squared error as the scoring metric. The training model includes four common categories of features: calendar data, lagged values, historical moving averages, and meteorological data, as detailed below. Forecasts are made based on these input features. Persistence forecast is used as the benchmark.

- Calendar data, time of the day and the year (using cyclic encoding), workday and non-workday indicators—including public holidays—and seasons.
- Lagged values, such as $y(d-24h)$, capture the CF value from the same time on the previous day, representing a 24-hour lag to reflect temporal data dependencies.
- Historical moving average, denoted as $MA\big(y(d-1\text{week}: d)\big)$, is the moving average of feature $y$ over one week.
- The average of the historical meteorological data for all of Switzerland is included in the training data, noting that real-time forecasting would necessitate real-time Swiss average weather forecasts. Using this feature depends on the availability of forecasted data.

Within the project, multiple Machine Learning (ML) algorithms are used and compared, including Extra Trees Regressor (ETR), Artificial Neural Networks (ANN), Elastic Net (Elnet), Random Forest (RF), Gradient Boosting Regressor (GBR), K-Nearest Neighbors (KNN), Linear Regression (LR), LASSO, Ridge regression, Support Vector Regression (SVR), and persistence forecast. As these algorithms are commonly chosen ones, detailed mathematical formulations of the algorithms are omitted in this report without impacting the reproducibility of results. Implementing these algorithms guides us in selecting the best-performing algorithm to be used for real-time forecasting. Both Sklearn[4] and Tensorflow[5] in Python serve as the primary tools for implementation.

### 2.2.3 Evaluation metrics

The error metrics considered are the Bias, Mean Absolute Error (MAE), Root Mean Square Error (RMSE), Normalized Root Mean Square Error (NRMSE), $R^2$ score, Mean Absolute Percentage Error (MAPE), and Normalized Mean Absolute Error (NMAE).

Bias measures the average tendency of the predictions to differ from the actual values. It is an indicator of systematic error in a model. The formula for calculating Bias is:

[4] https://scikit-learn.org/stable/
[5] https://www.tensorflow.org/

$$\text{Bias} = \frac{1}{n}\sum_{i=1}^{n}(\hat{y}^i - y^i)$$

where $y^i$ represents the actual value and $\hat{y}^i$ is the predicted value for the $i$-th data point, with $n$ being the total number of observations. A model with zero Bias is desirable, indicating no systematic error in the predictions.

The MAE accounts for the absolute difference between the estimated and the real values:

$$\text{MAE} = \frac{\sum_{i=1}^{n}|\hat{y}^i - y^i|}{n}$$

A lower MAE indicates better performance.

The RMSE heavily penalizes larger errors, with a lower RMSE representing better performance:

$$\text{RMSE} = \sqrt{\frac{\sum_{i=1}^{n}(\hat{y}^i - y^i)^2}{n}}$$

RMSE is relevant in forecasting result evaluation and is commonly used in other applications, such as evaluating modeling accuracy, which will be presented in later chapters.

The NRMSE is a normalized form of the RMSE, which more heavily penalizes larger errors:

$$\text{NRMSE} = \frac{100\%}{y^{\text{max}} - y^{\text{min}}}\sqrt{\frac{\sum_{i=1}^{n}(\hat{y}^i - y^i)^2}{n}}$$

where $(y^{\text{max}} - y^{\text{min}})$ is the range of actual values. A lower NRMSE represents better performance. The normalization allows for fair comparisons even when the values are not of the same magnitude.

The $R^2$ score, or the coefficient of determination, measures how well the variance in the dataset is captured by the model:

$$R^2 = 1 - \frac{\sum_{i=1}^{n}(\hat{y}^i - y^i)^2}{\sum_{i=1}^{n}(y^i - \bar{y})^2}$$

The $R^2$ score is bounded above by one but has no lower limit. Higher scores indicate better model performance. A score of zero corresponds to a model that only predicts the mean value of the test set.

The MAPE measures the accuracy of a forecasting method as a percentage. It is defined as:

$$\text{MAPE} = \frac{100\%}{n}\sum_{i=1}^{n}\left|\frac{y^i - \hat{y}^i}{y^i}\right|$$

A lower MAPE value indicates a higher accuracy of the forecast.

Normalized Mean Absolute Error (NMAE) is a variant of the MAE, with normalization allowing for fair comparisons even when the values are not of the same magnitude. It is defined as:

$$\text{NMAE} = \frac{100\%}{y^{\text{max}} - y^{\text{min}}}\frac{\sum_{i=1}^{n}|\hat{y}^i - y^i|}{n}$$

A lower NMAE value indicates better predictive accuracy.

## 2.3 Modeling and control

### 2.3.1 Control-oriented modelling

Control-oriented modeling uses a subspace identification technique, a system identification method (Armenise et al., 2018) used to construct models of dynamic systems from observed data. It offers a data-driven approach to modeling complex systems without requiring a detailed physical understanding of the system's internal processes. Note that additional modeling methods (i.e., Sparse Identification of Nonlinear Dynamics (SINDY) and Dynamic Mode Decomposition (DMD)) have also been explored and systematically compared in collaboration with the SWEET PATHFNDR project. For brevity, these results[6] are not shown in this report.

Consider a discrete-time LTI dynamical system with disturbance and output noise given by

$$\begin{aligned} x^{t+1} &= Ax^t + Bu^t + Ew^t, \\ y^t &= Cx^t + Du^t + v^t. \end{aligned}$$

where $x^t \in \mathbb{R}^{n_x}$, $u^t \in \mathbb{R}^{n_u}$, $y^t \in \mathbb{R}^{n_y}$, $w^t \in \mathbb{R}^{n_w}$, and $v^t \in \mathbb{R}^{n_y}$ are the states, inputs, outputs, disturbance, and output noise, respectively. The noise $v^t$ is considered to be zero-mean, independent, and identically distributed with a variance of $\sigma^2$.

The overall control-oriented modeling is summarized in Figure 4.

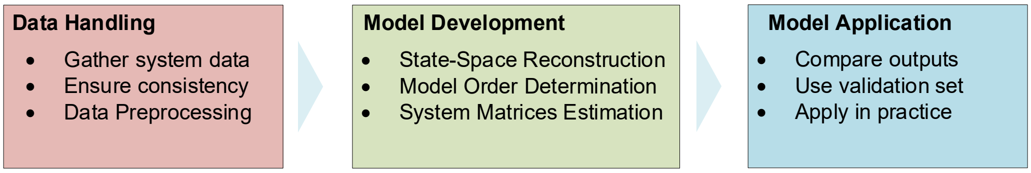


Figure 4. Control-oriented modeling using measurements.

The process starts with data handling, involving gathering input and output data from the system during its operation. This data must be consistently sampled to capture the system dynamics accurately. Data preprocessing is further carried out through interpolation and outlier removal. Afterward, state-space reconstruction, which uses the collected input-output data to reconstruct the system's state-space, is performed. Specifically, determining the model order and identifying the dimensionality of the state-space model are achieved using the Bayesian Information Criterion (BIC). Then, the system matrices (A, B, C, and D), which define the state-space model, are estimated. Model validation involves comparing the model's output with the actual system output using a separate validation dataset. Finally, the identified model is implemented for simulation and control.

More specifically, multiple subspace space identification algorithms, including N4SID (Van Overschee and De Moor, 1994), MOESP (VERHAEGEN and DEWILDE, 1992, p. 1), and CVA (Larimore, 1990) have been screened during the model development process. The screening results show that the N4SID algorithm performs best in our tasks in terms of RMSE. Therefore, N4SID has been chosen for the rest of this report. The SIPPY tool has facilitated the algorithmic implementation and comparison (Armenise et al., 2018).

### 2.3.2 Optimal control problem formulation

Closed-loop control involves solving optimal control problems, as compactly represented below in a receding horizon fashion. Upon solution, the first element in the optimal control sequence is applied. The compact formulation of the optimal control problem that is solved at every time step is given as follows.

[6] Brandes, Matthias. "Data-driven modeling of heat pumps and thermal storage units for MPC." Master's thesis, ETH Zurich, 2022.

$$
\begin{array}{lll}
\min_{u^t} & J_u(u^t) & \\
\text{s.t.} & x^{t+1} = Ax^t + Bu^t, & \forall\, t \\
& y^t = Cx^t + Du^t, & \forall\, t \\
& u^t \in \mathcal{U}^t, y^t \in Y^t, & \forall\, t
\end{array}
$$

where $u^t$ denotes the decision variables, $J_u(u^t)$ is the total cost, $\mathcal{U}^t$ and $Y^t$ are the operating limits of inputs and outputs, respectively. An illustrative input example includes the thermal power constrained by hardware limitations, while a corresponding output example comprises the water tank temperature restricted by minimum and maximum operating temperatures. During closed-loop control, the Kalman Filter is used for state estimation. Upon solution, the first element of $u^t$ is sent to the infrastructure for actuation. This control scheme is commonly known as Model Predictive Control (MPC). Note that the process presented here can be further simplified to improve scalability and facilitate the timely implementation of DSM to more comprehensive building stock, as described in sub-chapter 2.5.

For NEST, two configurations were considered: 1) PV and energy hub, and 2) PV, energy hub, and a stationary battery. For K3, the cost functions consider the carbon footprint at the building level, including all assets behind the meter. That is to say, PV, CHP, HPs, and fixed loads were considered in the optimization.

## 2.4 Flexibility quantification and provision

The flexibility envelope concept is used in this report. Initially, the upper and lower energy bounds are identified by energizing the building to its extremes, which consists of solving two optimization problems as follows:

$$
\begin{aligned}
J_{\text{upper}} &= \min_{u,\delta} \; -w^\intercal u + w_\delta \cdot \| \delta \|^2, \\
J_{\text{lower}} &= \min_{u,\delta} \; w^\intercal u + w_\delta \cdot \| \delta \|^2,
\end{aligned}
$$

where $u$ is a vector of the active power of all components, $w$ is a vector of weights, $\delta$ is a vector of slack variables introduced to ensure feasibility and $w_\delta \in \mathbb{R}_+$ is the corresponding weight.

Optimization constraints include the dynamics of each component, power, and energy capacities, state limits, and mutual exclusiveness of charging and discharging. The respectively obtained $u$ gives the upper and lower energy bounds. The optimal decisions obtained give rise to the upper and lower energy bounds. The feasible power levels and the corresponding maximum sustained duration can be derived using the procedure shown in Figure 5. When applying this derivation in all the lead times within the horizon, a flexibility envelope spanned by lead time, power levels, and maximum sustained duration is obtained. In real-time applications, the entire quantification process is periodically repeated to account for the most recent observations. The interaction between flexibility provider and procurer in terms of information flow is illustrated in Figure 6. Detailed mathematical formulations are elaborated in (Cai and Heer, 2021).

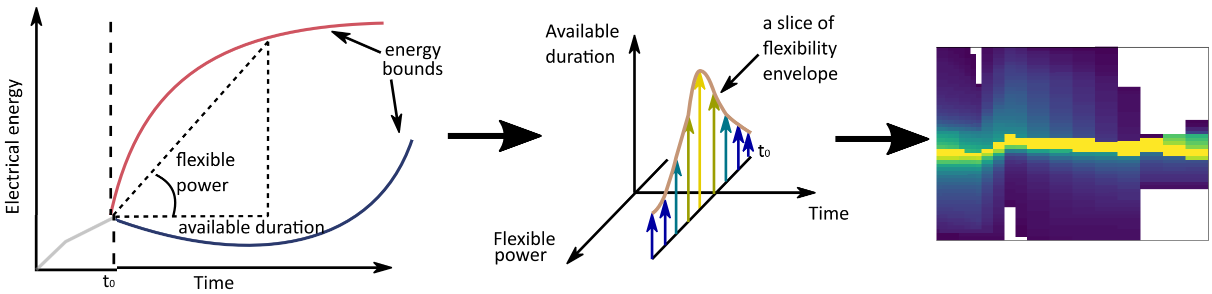


Figure 5. Calculate maximal sustainable duration by identifying energy bounds and deriving sustainable duration of chosen power levels (Hekmat et al., 2023).

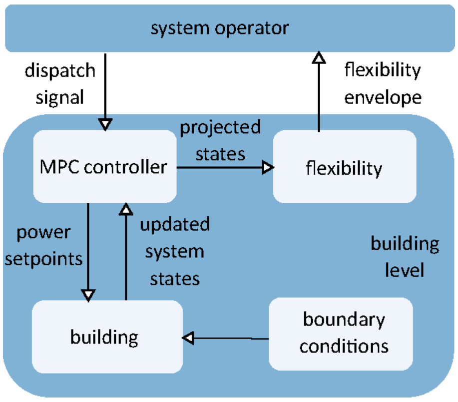

Figure 6. Illustration of the information flow among the building, the controller, and the system operator (Cai and Heer, 2021).

This flexibility quantification and provision scheme is crucially dependent on the predictive control schemes presented in sub-chapter 2.3 and sub-chapter 2.5.

## 2.5 Data-driven predictive control for enabling DSM

The International Energy Agency (IEA) estimates that one billion households and eleven billion smart appliances could actively participate in global demand response programs by 2040, which can be seen as a subcategory of DSM (International Energy Agency, 2017). The method presented below contributes to reducing technical implementation barriers of DSM, supporting scalable and fast uptake. Specifically, it distinguishes from the method introduced in sub-chapter 2.3 in that there is no parametric model, effectively eliminating the modeling efforts. The rest of sub-chapter 2.5 revisits the theoretical background of data-driven predictive control and presents a stochastic indirect data-driven predictive control scheme with constraint tightening to ensure that constraints are satisfied with a predefined probability. More details of the method presented here can be found in (Yin et al., 2024).

In conventional MPC algorithms, such as that in sub-chapter 2.3, the output is predicted and controlled by iteratively propagating the state-space model, assuming the knowledge of the model parameters $(A, B, C, D, E)$ is available. In data-driven predictive control, however, no prior knowledge about the parameters is required, but a matrix of input-disturbance-output trajectory data.

$$Z = [z_0^d \quad \cdots \quad z_{M-1}^d]$$

has to be collected from historical data or high-fidelity simulation, where each column

$$z_i^d = \text{col}\left(u_{t_i}^d, \dots, u_{t_i+L-1}^d, w_{t_i}^d, \dots, w_{t_i+L-1}^d, y_{t_i}^d, \dots, y_{t_i+L-1}^d\right)$$

is a length-$L$ trajectory of the system. This matrix is referred to as the signal matrix. Using Willems' fundamental lemma in the behavioral system theory, a nonparametric input-output mapping can be directly obtained from the signal matrix $Z$ when no noise is present, i.e., $v_t = 0$. The method is summarized as follows.

With sufficiently persistently exciting inputs, the range space of $Z$ contains all possible trajectories of the system. Let $L = L_0 + L'$, and $L_0$ be no smaller than the observability index of the system. Define a partition of $Z$ as

$$Z = \text{col}\{U, W, Y_p, Y_f\} = \text{col}\{\Psi, Y_p, Y_f\},$$

where $U \in \mathbb{R}^{n_u L \times M}$, $W \in \mathbb{R}^{n_w L \times M}$, $Y_p \in \mathbb{R}^{n_y L_0 \times M}$, $Y_f \in \mathbb{R}^{n_y L' \times M}$, and $\Psi \in \mathbb{R}^{(n_u+n_w)L \times M}$. The noise-free signal matrix satisfies the rank condition

$$\text{rank}(Z) = \text{rank}\big(\text{col}\{\Psi, Y_p\}\big) = (n_u + n_w)L + n_x.$$

Then, the $L'$-step-ahead output predictor $\mathbf{y}^t = (y_k)_{k=t}^{t+L'-1}$ at time $t$ can be constructed from the past input sequence $\mathbf{u}_{\text{ini}}^t = (u_k)_{k=t-L_0}^{t-1}$, the future input sequence $\mathbf{u}^t = (u_k)_{k=t}^{t+L'-1}$, the disturbance sequence $\mathbf{w}^t = (w_k)_{k=t-L_0}^{t+L'-1}$, and the past output sequence $\mathbf{y}_{\text{ini}}^t = (y_k)_{k=t-L_0}^{t-1}$ by solving the linear equations

$$\begin{bmatrix} \Psi \\ Y_p \end{bmatrix} g = \text{col}\{\mathbf{u}_{\text{ini}}^t, \mathbf{u}^t, \mathbf{w}^t, \mathbf{y}_{\text{ini}}^t\},$$

where $g \in \mathbb{R}^M$ is an intermediate vector. The output prediction is then given by

$$\mathbf{y}^t = Y_f g.$$

In this work, optimal controllers are designed to minimize given control objectives $J_u(\mathbf{u}^t)$, e.g., carbon footprint, subject to input and output constraints $\mathbf{u}^t \in \mathcal{U}^t$, $\mathbf{y}^t \in \mathcal{Y}^t$ at time $t$. Similar to standard MPC, the scheme is applied in a receding horizon fashion.

In practice, however, when noise and uncertainties exist, the above algorithm cannot be directly applied. In this work, two sources of uncertainties are considered. 1) Noise in output measurements and 2) Uncertainties in online disturbance measurements and predictions. In the publication (Yin et al., 2024), indirect data-driven predictive control is extended to provide stochastic control using techniques similar to those in stochastic MPC. This leads to the following stochastic control problem:

$$\begin{aligned} \min_{\mathbf{u}^t} \quad & J_u(\mathbf{u}^t) \\ \text{s.t.} \quad & \mathbf{y}^t \sim \mathcal{F}(\mathbf{u}_{\text{ini}}^t, \mathbf{u}^t, \bar{\mathbf{w}}^t, \bar{\mathbf{y}}_{\text{ini}}^t; Z), \\ & \mathbf{u}^t \in \mathcal{U}^t, \quad \mathbb{P}(h_i^t \mathbf{y}^t \le q_i^t) \ge p, \qquad \forall\, i = 1, \dots, n_c, \end{aligned}$$

where $\mathcal{F}(\cdot)$ is the stochastic data-driven predictor. Due to the potentially unbounded noise, the output constraints cannot be satisfied robustly, but only with a high probability $p$ as chance constraints for constraint $i$.

## 2.6 Flexibility at the national scale

The development of flexibility quantification methodology of buildings, described in sub-chapter 2.4, has been used to investigate the spatial and temporal distribution of space heating demand flexibility at the national level, with granularity at the community level. The flexibility here is defined as the duration the building's power can be curtailed without compromising comfort levels. This logic resembles the ripple control strategy. Therefore, all the developed methods are combined to provide insights into potential impacts at the system level.

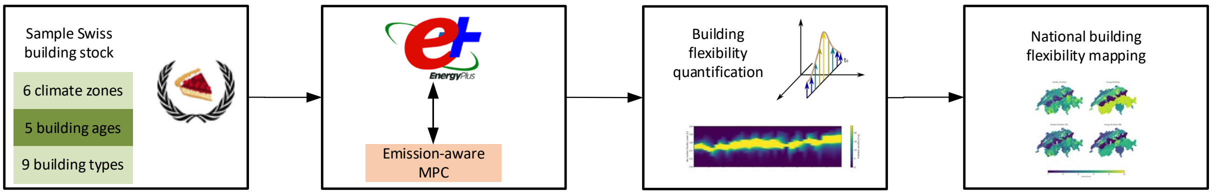

Figure 7. Workflow of bottom-up flexibility quantification in four steps. The first step includes selecting buildings for investigation. The second step includes creating input files for EnergyPlus simulation and an interface for real-time data exchange. The third step concerns flexibility quantification at the individual building level. Lastly, the last step maps flexibility potential to different regions.

Since energy flexibility is highly dependent on initial conditions, it is assumed that GHG emission-aware predictive controllers are used as default controllers in all buildings to provide the intial conditions. The resultant building states (e.g., zone temperatures) are used as initial conditions to quantify energy flexibility. Such baseline predictive controllers are implemented using co-simulation, where high-fidelity models of the selected buildings are implemented in EnergyPlus, and controllers are implemented in Python. The information exchange at runtime is facilitated with EnergyPlus Runtime API. Furthermore, the overall workflow is summarized in Figure 7. The first step includes selecting buildings for investigation. More specifically, we consider 6 climate zones, 5 building ages, and 9 types. (Eggimann et al., 2022) developed a building database for Switzerland containing approximately 2.3 million buildings and other built elements (e.g., silos) that serves as a basis for performing simulation experiments and to up-scale individual building simulation results on the national scale. Due to computational limitations, it is not feasible to simulate every Swiss building, and a representative selection of buildings must be made. Single-family houses, multi-family houses, and offices account for almost 86% of the total building stock. Therefore, focusing on these selected building types allows for abstracting national building stock. The second step includes creating input files for EnergyPlus simulation using CESAR-p (Orehounig et al., 2022) and an interface for real-time data exchange. This step uses the carbon footprint profile provided using the method in Chapter 2.2. The third step concerns flexibility quantification at the individual building level. Lastly, the last step maps flexibility potential to different regions. Mapping with the information of the geographical distribution of buildings, high spatial resolution can be obtained.

# 3 Results and discussion

This chapter begins by presenting the results of analyzing the historical CF signal for the Swiss electricity mix and the corresponding forecasting performance evaluation. A detailed analysis of field measurements within the reference year is then provided to give an overview of the existing operation patterns. Additionally, the chapter summarizes the findings for control-oriented modeling, flexibility identification, and simulation-based performance comparison. Following this, experimental results on emission-aware predictive control are discussed. Furthermore, the chapter explores additional data-driven pipelines aimed at removing technical barriers for DSM through experiments at NEST. Finally, the chapter leverages all the methodological development and shows an example of the national distribution of space heating demand flexibility, which may be exploited with ripple control infrastructure.

## 3.1 Forecasting the temporal profile for the carbon footprint

This chapter summarizes the results related to the method described in sub-chapter 2.2. Figure 8 shows an overview of the historical CF signal for the Swiss electricity mix from 2017 to 2022. The carbon footprint fluctuations can be observed throughout the year and also happen during the days (not visible in the figure below).

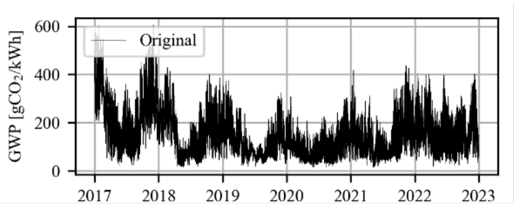


Figure 8. Overview of the CF signal for the Swiss electricity mix.

To understand the relevance of the CF forecast, we first analyzed carbon footprint reduction potentials in ideal conditions: perfect forecast and load shifting. The results summarized in Figure 9. Carbon footprint reduction potentials as the horizon increases indicated an initial phase of rapid increase, suggesting that with each incremental unit increase in the forecasting horizon, there was a significant gain in the potential reduction of GHG emissions. However, as the horizon expanded beyond a certain point, the reduction potential increase rate began to slow down and showed a saturation state. Being technology-agnostic, this insight can apply to thermal loads considered in this report via advanced control and other domestic appliances once users know their preference for the delayed start.

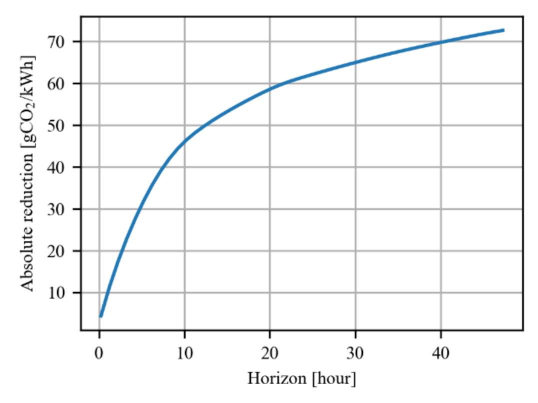


Figure 9. Carbon footprint reduction potentials as the horizon increases: a technology-agnostic assessment in ideal conditions.

Due to the changing patterns across different years, the results presented in Figure 9 were further analyzed for individual years. The annual distribution of reductions is summarized in Figure 10. While there is no clear pattern in absolute reduction potential, the mean values of normalized potential from 2017 to 2022 showed a noticeable upward trend, increasing from 19.60% in 2017 to 24.50% in 2022. The variability of the data also showed an increasing trend indicating a general shift towards higher reduction potentials.

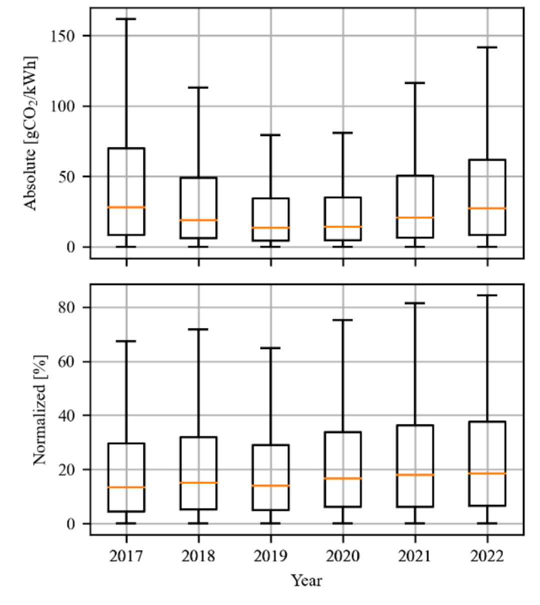


Figure 10. Box plots of absolute and normalized carbon footprint reduction potentials by year.

The rest of this sub-chapter focuses on summarizing the performance of forecasting algorithms. To create a forecasting algorithm, we used the different outputs of the codes from WP1 (i.e., outputs of the EcoDynElec package). We also considered data on historical weather forecasts, solar irradiation levels, production capacity, and typical demand levels in Switzerland. We started with feature analysis to determine the potential impacts of considered inputs on the predicted CF. The training datasets spanned from January 1, 2017, to December 31, 2019[7].

Figure 11 shows the Pearson correlations of the standardized input features with the CF results (provided with the GWP indicator) over the training datasets. Historical and recent CF values strongly correlated to the predicted CF, as shown in the ranking of lagged and moving average CF features, with scores from 0.84 to 0.71. Weather features, including temperature and solar radiation, exhibited moderate negative correlations with the predicted CF, irrespective of the country or lag time. Summer and winter had moderate correlations with the predicted CF values in a day-ahead horizon. Conversely, spring and autumn had weak negative and positive correlations. This difference was due to more pronounced summer and winter weather than spring and autumn. Day and night features had a weak positive and negative correlation with the predicted CF, which can be explained by the critical dependence of day and night conditions on the seasons and across the year. Among the additional tested features, electricity consumption levels and the intraday price in Switzerland had moderate and weak positive correlations, respectively. Furthermore, the electricity demand (indicated by de_con in Figure 11) and the electricity price in Germany (indicated by de_price in Figure 11) had very low influences on the Swiss CF (shown by weak correlation scores below 0.10).

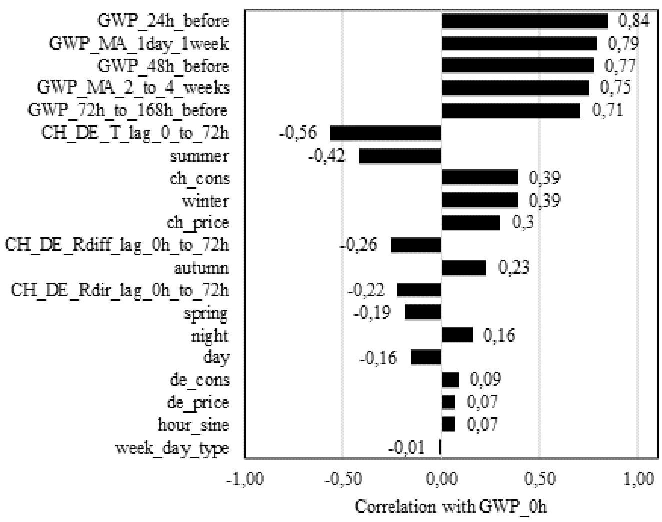


Figure 11. Impacts of input features on the predicted CF signal.

The effect of input feature selections on CF prediction accuracy at time 0 was examined across six different input feature selections. The results stemmed from a Ridge regression algorithm trained and tested on the same specific training datasets. Table 2 shows the R2 scores of the output CF for the different input feature selections. The best-performing selection was "Complete" with a score of 0.784, including recent and historical CF values and the current contextual data calendar, CH/DE weather, national consumption, and price. Conversely, the worst R2 value of 0.497 is obtained without GWP data and only with current contextual data, namely "No GWP". Interestingly, feature selections that include only GWP data, namely "Recent GWP only" and "Only GWP", exhibited R2 values close to the best performing "Complete" selection. In practice, using only historical GWP values could be a viable choice to minimize the number of input features and the complexity of the forecasting approach while

[7] This time range is selected only during feature analysis due to unavailability of certain data after 2020, such as weather data outside Switzerland. However, this range is chosen uniformly throughout the feature analysis.

maintaining good prediction performance. Furthermore, the "Recent" selection, which includes only lagged 24h GWP data and current contextual data, performs close to the more informed model regarding historical GWP trends. Overall, the results of this performance analysis show that using recent GWP data is critical for reliable real-time prediction, and including current contextual information further improves the prediction by ~5%.

Table 2. R2 scores of six different input feature selections. "Y" indicates selection, and "-" indicates absence of feature.

| Input feature | Initial | Complete | No GWP | Recent GWP only | Only GWP Recent | Lagged GWP Recent |
|---|---|---|---|---|---|---|
| Lagged GWP 24h to 168h | 24h to 168h | 24h to 168h | - | 24h | 24h to 168h | 24h |
| Moving average GWP | Y | Y | - | - | Y | - |
| Calendar | Y | Y | Y | - | - | Y |
| CH/DE weather | Y | Y | Y | - | - | Y |
| CH/DE consumption and price | - | Y | Y | - | - | Y |
| R2 score | 0.773 | 0.784 | 0.497 | 0.707 | 0.743 | 0.752 |

For computational purposes, the rest of the report presents results using data from January 1, 2020, to December 31, 2022, and the "Only GWP Recent" feature will be considered. The split ratio for the input CF datasets is 80% for training and 20% for testing. The CF dataset was split into the training set and the test set, where the training dataset accounted for 80% of the data. The test dataset was exclusively used for the evaluation of the model's predictive performance. No shuffling was used, and the test dataset included the data at the end of the selected period.

A detailed summary of the performance comparison among different algorithms is provided in Table 3. Summary of performance across different forecasting algorithms. The Lasso, LR, and Ridge models exhibited consistently strong performance across all metrics, suggesting they are reliable for prediction in this context. They maintained low RMSE and high R2 values. The Persistence model had the weakest performance, with the highest errors and a negative R2 value, rendering it unsuitable for our forecasting task. The ensemble methods such as ETR, GBR, and RF showed moderate performance. While they did not match the best models, they still outperformed the Persistence model significantly. The ANN model showed a high R2 value. However, it did not outcompete the simpler model despite its complexity. In summary, the Lasso, LR, and Ridge models are recommended due to their strong and consistent performance for such a task. The results agree with those obtained by (Bokde et al., 2021), which report a low gain in performance using a more sophisticated approach than linear models for Switzerland.

Table 3. Summary of performance across different forecasting algorithms.

| Metric | Persistence | ANN | Elnet | ETR | GBR | KNN | Lasso | LR | RF | Ridge | SVR |
|---|---|---|---|---|---|---|---|---|---|---|---|
| Bias [gCO2/kWh] | 154.98 | 6.55 | 21.56 | 40.5 | 43.11 | 18.21 | 2.02 | 1.38 | 38.24 | 1.35 | 9.11 |
| MAE [gCO2/kWh] | 154.98 | 33.52 | 47.16 | 51.51 | 52.66 | 42.98 | 32.62 | 32.56 | 50.22 | 32.57 | 34.96 |
| RMSE [gCO2/kWh] | 167.02 | 42.1 | 60.05 | 65.76 | 67.93 | 55.52 | 41.16 | 41.14 | 64.82 | 41.1 | 43.71 |

| | | | | | | | | | | |
|---|---|---|---|---|---|---|---|---|---|---|
| R2 [-] | −6.19 | 0.54 | 0.07 | −0.11 | −0.19 | 0.21 | 0.56 | 0.56 | −0.08 | 0.56 | 0.51 |
| NMAE [%] | 41.18 | 8.91 | 12.53 | 13.69 | 13.99 | 11.42 | 8.67 | 8.65 | 13.34 | 8.65 | 9.29 |
| NRMSE [%] | 44.38 | 11.19 | 15.96 | 17.47 | 18.05 | 14.75 | 10.94 | 10.93 | 17.22 | 10.92 | 11.61 |
| MAPE [%] | 100 | 26.23 | 33.89 | 31.73 | 31.58 | 30.2 | 26.22 | 26.27 | 31.09 | 26.3 | 26.39 |

Additionally, LR, Ridge, and Lasso forecast CF signals with an NRMSE lower than 15%. We only needed to use the data from the last 28 days to reach such performance. With that in mind, the automated data-gathering options of WP1 were limited in time to the historical data from the last two months. This kind of performance was deemed sufficient to start using the forecasting method to create CF signals that would guide the DSM of the buildings.

As for real-time forecasts, Figure 12 illustrates the overall implementation procedure and information flows. Automated data-gathering algorithms have been created to acquire the latest information from the ENTSO-E platforms. These algorithms connected to the FTP server of ENTSO-E and downloaded the raw data that was needed as input for the 15-minute algorithms (i.e., EcoDynElec). It was then possible to calculate the CF profile for the Swiss electricity mix automatically for the last two months, which was required to forecast the CF profile for the next 24 hours. The combination of the automated data gathering feature and the 15-minute CF assessment algorithms was launched every hour when ENTSO-E released new statistics on electricity production and exchanges in European countries. These data were then coupled with the most performing algorithm identified previously to have runtime forecasts.

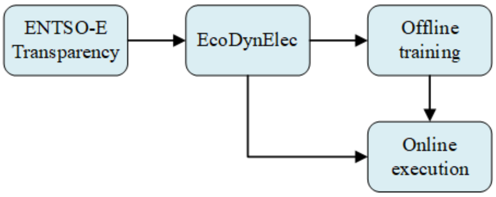


Figure 12. The overall real-time forecasting system setup procedure involves data retrieval, GWP calculation, offline training, and online execution.

A data quality issue was identified during the project. The calculated “most recent GWP” feature using retrieved data from the ENTSO-E platform varied over time, and the statistics of the variations, presented in standard deviation, are summarized in Figure 13. We hypothesize that the database updated its data over time due to unsynchronized datastreams to the ENTSO-E platform. Therefore, the platform constantly changed historical values, leading to the observed variations and null values.

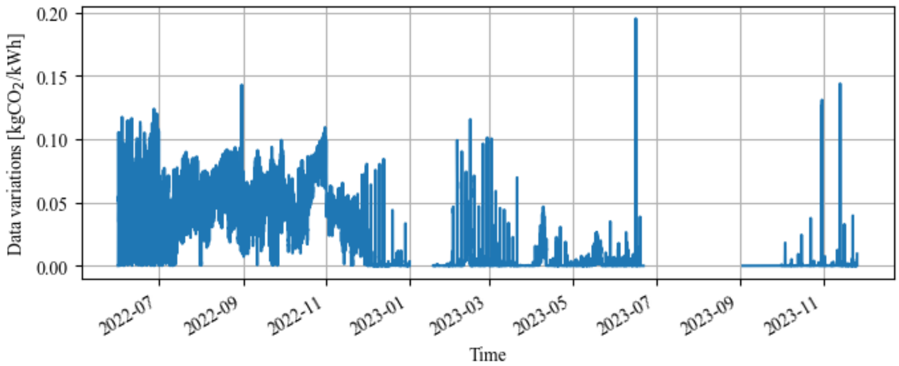


Figure 13. Variations of calculated “most recent GWP” parameter using retrieved data from the ENTSO-E platform.

Nonetheless, the real-time forecast has been operational and made externally accessible through MQTT[8]. In this regard, an EU Horizon project[9] has requested and received the service to optimize data-center scheduling according to the electricity CF. Further descriptions of their application and results fall out of the scope of this report.

## 3.2 Measurement campaign for the reference year

This chapter summarizes the analysis of historical data for both NEST and K3, focusing on existing operational patterns and potential issues, such as voltage band violations, that DSM can contribute to resolving, although they could not be resolved within this project's scope.

### 3.2.1 Location NEST

Data on electricity consumption from the NEST building has been collected and stored from 2017 onwards. The data can be read via interfaces like web applications, direct database access, or APIs. An overview of the components considered in this project can be found in Figure 55. The current operation of the heat pumps is demand-oriented and not predictive. For past projects, the mode of operation was changed, e.g., in (Bünning et al., 2020) to identify and offer ancillary services with a hierarchical controller setup incorporating thermal demand, storage, and the operation of one heat pump. The energy hub at NEST has been physically upgraded with more buffer tanks, and the data of the new system configuration have been collected since November 2022. This upgrade increased the level of energy flexibility at NEST. Measurements of voltage at NEST over two years are shown in Figure 3. The voltage was controlled within desired ranges in contrast to the voltage profile observed at K3, as shown in the yearly report 2021, sub-chapter 3.2.2. The more stable voltage profile in NEST was mainly due to smaller sizes of PVs at the site and an over-sized network.

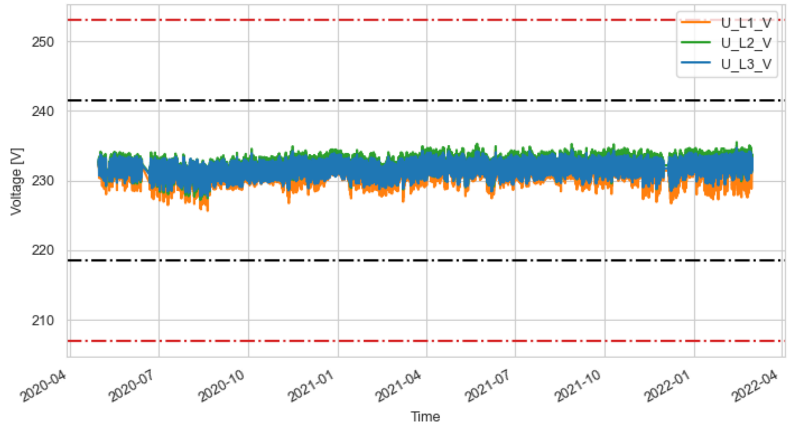


Figure 14. Voltage measurement at NEST showing each phase and specification bounds (dashed black) and critical bonds (dashed red).

SFOE expressed interest in adding EV charging integration to the project's DSM. To analyze the potential of this integration, measurement data from a charging station at Empa (located at the MOVE demonstrator, connected to the same electrical grid as NEST; measurement and data collection were done by the same systems as NEST) was retrieved and analyzed. The log files from the charging station were parsed to extract info on the charging sessions. The data presented in this chapter were collected before COVID-19, indicating energy flexibility in nominal operation. We extracted info such as the number of cars plugged in, their state of charges (SOCs) at arrival and departure, and the maximum active power the vehicle can absorb. Data showed that EVs arrived at this charging station

[8] https://mqtt.org/
[9] https://eco-qube.eu/

with a wide range of SOCs, as Figure 15 and Figure 16 show. As for the SOC at departure, it was more consistent; apart from a few outliers, most vehicles left with at least a SOC of 80%.

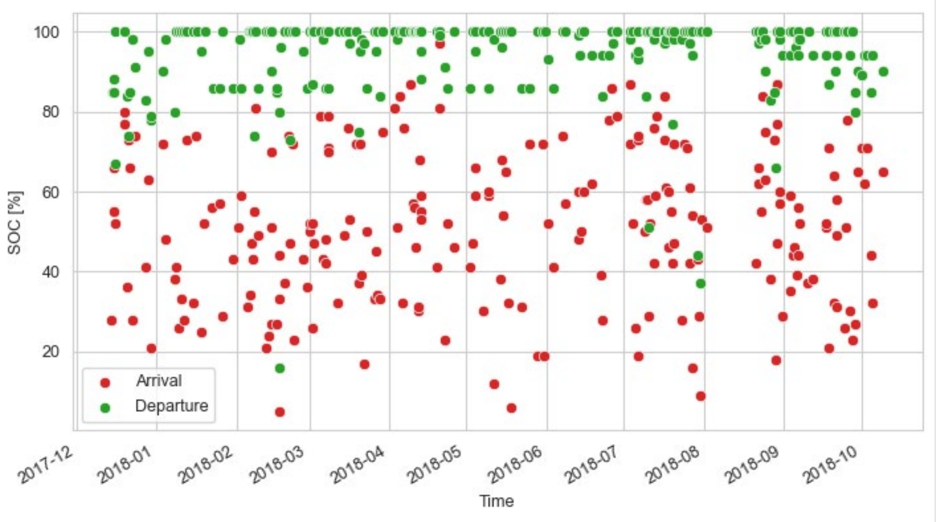


Figure 15. Scatter plot of arrival SOC and departure SOC for the charging station at the MOVE demonstrator.

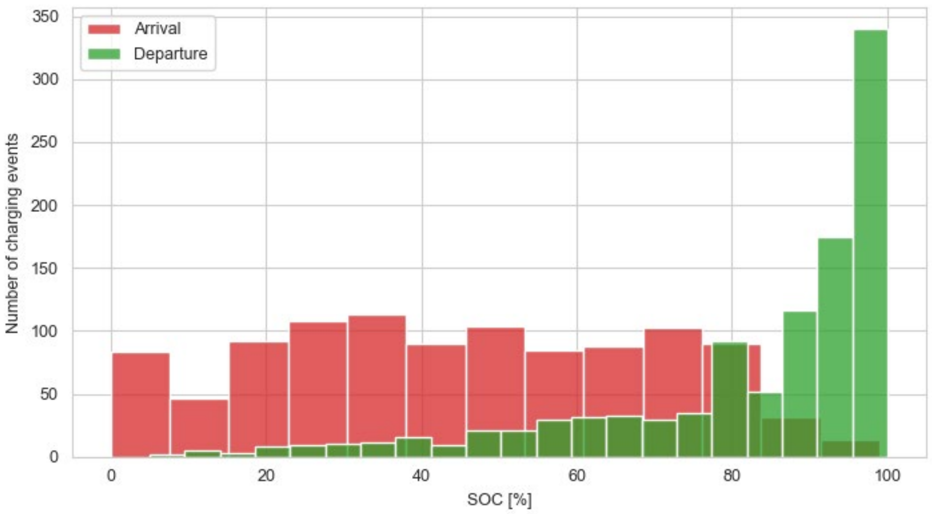


Figure 16. Histogram of arrival SOC and departure SOC at the MOVE demonstrator.

The daily and weekly patterns of EV arrival and departure are summarized in Figure 17. During workdays, we can observe a pattern associated with working schedules: arrival/plugged-in time concentrated in the early morning and departure/unplugging in the evening; during weekends, we can observe a decrease in charging events and a temporal shift in arrival and departure. Such patterns were likely a combined effect of free charging at this site, vehicles from tours/visitors, and the schedules of researchers.

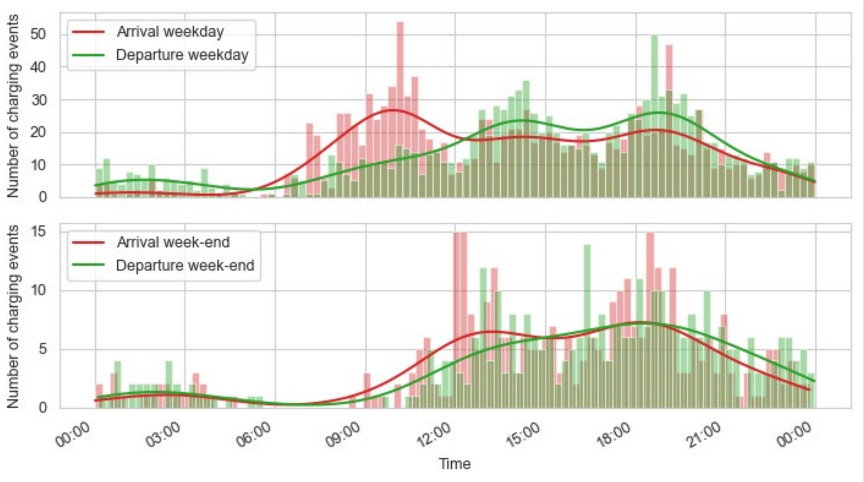


Figure 17. Histogram of the arrival and departure times.

Both Figure 15 and Figure 16 provide an overview of EV's energy consumption and inform on the scale of potential impacts (e.g., indirect GHG emissions). However, idle time was needed to assess their flexibility when EVs were available for load shifting. This is summarized in Figure 18; we defined idle time as the duration between being fully charged and unplugged vehicles. We can observe that most of the time, an EV was unplugged shortly after being fully charged. The idle duration was, on average, 43 minutes. This indicated minimal load-shifting capability and potential reduction of indirect GHG emissions. Because the exogenous factors, such as the price and the CF of electricity, were unlikely to change dramatically within such a short time window.

One reason for this was the limited number of charging stations on site. When an EV was charged fully, the owner got a notification, and he/she may unplug the EV to make way for other colleagues. Therefore, flexibility levels are expected to increase when more charging stations are made available and EVs remain plugged in for longer periods of time. Other charging stations at Empa are currently under construction, and more flexibility could be expected in the future.

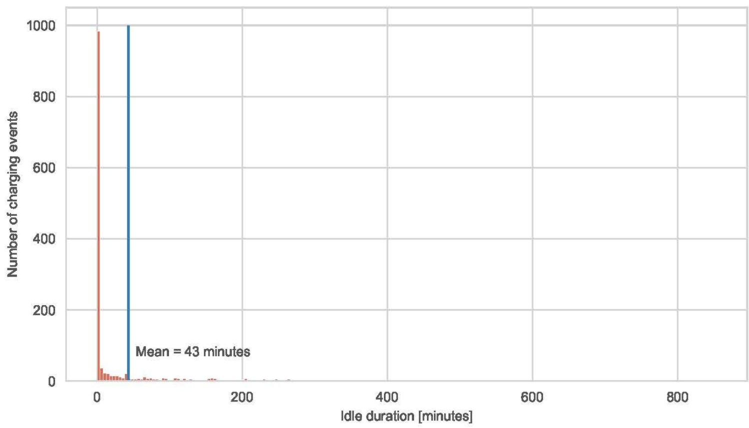


Figure 18. Histogram of the idle duration of vehicles parked at the MOVE demonstrator.

### 3.2.2 Location K3

The electrical energy consumption was attributed to space heating (SH), space cooling (SC), domestic hot water (DHW), and other electrical loads, as shown in Figure 19. The electrical consumption for thermal comfort, namely space heating, space cooling, and domestic hot water, accounts for 36%. The relatively minor share of thermal loads in total energy consumption may have contributed to the modest reduction in carbon footprint when considering the building's overall energy use in the controller design.

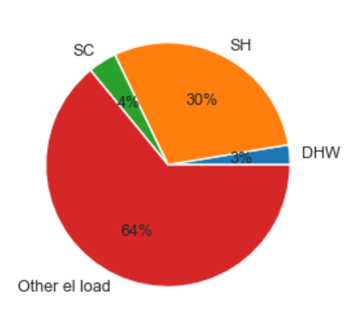


Figure 19. Annual electrical energy consumption decomposed by end uses in the K3 building

Additionally, we have analyzed the data of individual systems, including HP, PV, CHP, and storage tanks. An overview of the components considered in this project can be found in Figure 56. Generally, the analysis includes 1) data cleaning, 2) synthesizing missing data (e.g., the PV installation has been partially shut down), and 3) visualization and identification of potential issues in operation. Example results of the analysis of K3 are given in the rest of this chapter. The overvoltage phenomenon due to excessive PV output is shown in Figure 20 with both duration curves and time series. We can observe that overvoltage events occurred 6-9% of the time and happened during the middle of the day when solar irradiance was high.

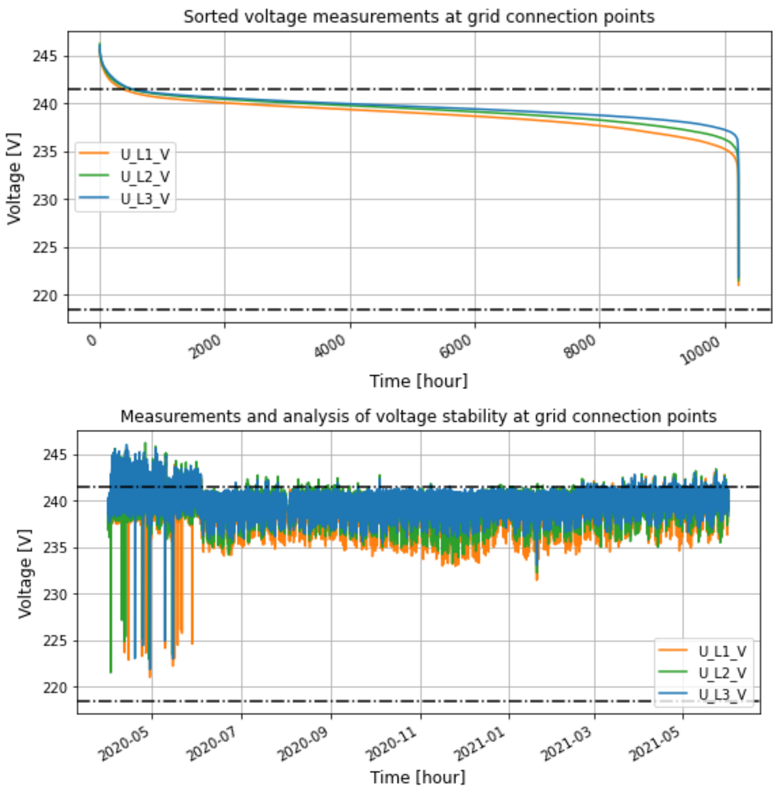

Figure 20. Analysis of grid voltage stability. Top plot: sorted voltage measurements at the grid connection points, and the dashed lines indicate voltage limits (1±0.05 pu.). Bottom plot: time-series view of the voltage measurements at three phases over one year.

In view of this voltage challenge, we designed an algorithm to assess the benefits of ideal HP electrical load shifting to improve PV self-consumption. We assumed perfect HP electrical load prediction and then shifted the HP electrical load freely to minimize the electricity export from the building. With the flexibility from unconstrained load shifting, PV self-consumption can be improved. Note that the algorithm relied on the perfect forecast of PV output, HP usage, and consumption of other electric loads. Hence, the presented results were theoretical, and the realized benefits in practice will be lower. Nonetheless, we can see the benefits of shifting the HP consumption by including predictive knowledge. The horizon of such predictive knowledge had substantial impacts and a sensitivity analysis is summarized in Figure 21 and Figure 22.

We can observe that the benefits increase steadily as the length of the forecast horizon increases in Figure 21. More specifically, when the horizon increased from 0 to 5 hours, the self-consumption benefits increased the most. After that, the benefits reached a plateau, with 5 MWh of total HP electricity usage from the PV installation. When HP electrical load shifting was not considered (i.e., horizon is 0), only 3 MWh of the electricity usage came from the PV installation.

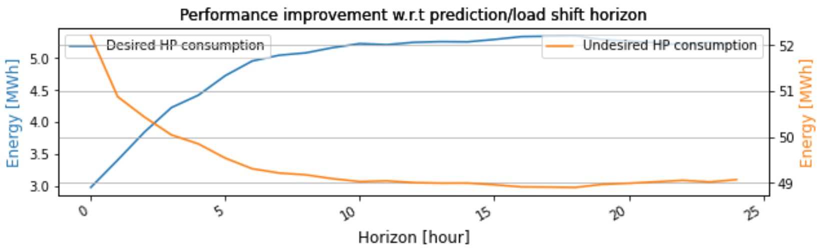


Figure 21. Improvement of self-consumption by shifting HP electricity usage with realized PV output. The "desired HP consumption" means HP uses electricity when the entire building is exporting electricity to the grid. The "undesired HP consumption" means the rest.

The above results were based on the measurements when PV was in partial operation. With the synthesized PV output (by combining the machine-learning technique with brightness sensors mounted on the walls), we further examined the scenario where the entire PV installation would operate. A similar sensitivity analysis is shown in Figure 22, and we can observe a similar trend. However, the plateau was reached when the horizon was around 12 hours. Without HP load shifting, 9.5 MWh of its total electricity consumption could have been supplied by the PV installation. The value increased to around 12.4 MWh (+30%) when accounting for load shifting.

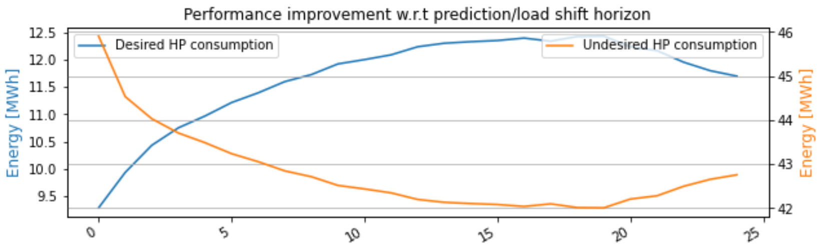


Figure 22. Improvement of self-consumption by shifting HP electricity usage with synthesized PV output. The "desired HP consumption" is the consumption that can be shifted to periods when the entire building is exporting electricity to the grid. The "undesired HP consumption" means the rest of the energy usage from HP.

## 3.3 Modeling, control, and flexibility in buildings

This part of the results has been derived using methods in sub-chapters 2.3 and 2.4. We derived models based on the collected measurement data. Specifically, we covered linear models of CHP and HPs, data-driven day-ahead forecasts of cooling and heating demands, fixed load, hot water usage, PV output and carbon intensity of electricity, and models of heat and cold storage tanks. All models were obtained with a sampling time interval of 15 minutes. We identified the parameters of the model structures by minimizing errors of n-step ahead predictions. As a predictive controller was envisioned, we presented the accuracy concerning different lead times, i.e., different prediction steps. Such accuracy metrics ultimately determined the choice of time horizon for the predictive controller. A long horizon of up to 24 hours could allow the controller to incorporate the forecast of PV output. However, the modeling accuracy would decrease simultaneously.

### 3.3.1 Modeling ehub of NEST

The ehub of NEST, as illustrated Figure 23, was modeled with linear models. Modeling errors for different lead times are summarized in Figure 24.

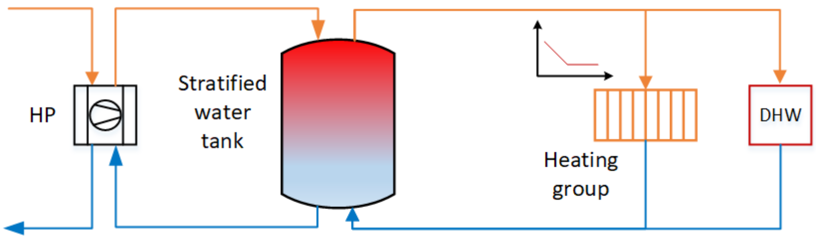


Figure 23. Simplified overview of the ehub at NEST.

The energy hub at NEST had several upgrades throughout the project, and there were other energy sources in addition to the HP-based system shown in Figure 23. For example, the district heating network of the Empa campus was also used to supply the heating demand of NEST when HP could not meet the demand. This is due to the incremental feature of NEST, in which more and more units get installed.

The modeling performance is assessed and summarized in Figure 24 for the low-, medium- and high-temperature thermal distribution grid within the building. The performance is presented for both multi-step ahead prediction errors and time-series views. In all cases, we can observe that prediction errors increased initially and saturated quickly. The modeling errors were relatively low compared with the original data's standard deviation (SD).

The operating temperature medium-temperature network at NEST was confined within a smaller range than that of K3. The upper limit of temperature was lower because a high temperature could prevent the usage of solar thermal and may negatively impact the wooden floor. Therefore, the temperature was constrained in a fixed range, rather than following the heating curve concept, in which temperature could go up to 45 degrees at K3 (note that, if the CHP is used, the temperature can rise much higher).

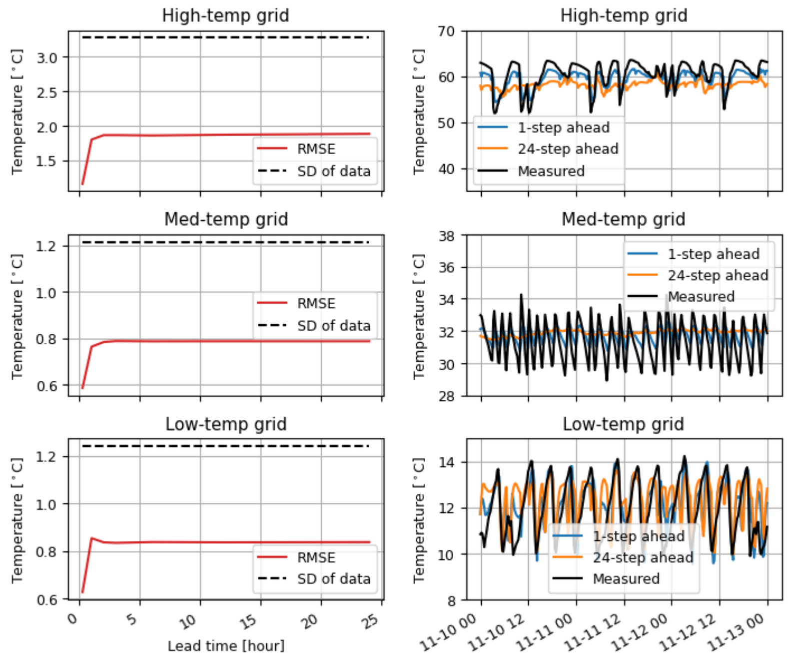


Figure 24. Assessment of modeling performance of the energy hub at NEST. Left: multi-step ahead prediction error. Right: time-series view of the model performance on selected days.

The flexibility from the perspective of the existing ripple control infrastructure was quantified and summarized in Figure 25. Flexibility from the perspective of the existing ripple control infrastructure. Top: the duration that NEST medium temperature grid can be virtually disconnected. Medium: ambient temperature. Bottom: thermal load measurements., along with ambient temperature and thermal demand measurements. In other words, flexibility here implies the duration that the energy hub power can be curtailed without impacting user comfort levels. This flexibility was obtained using the flexibility envelope concept described in sub-chapter 2.4, where the duration metric can be obtained by cutting the flexibility envelope. The tank temperature operating range was between 28 °C and 35 °C. We can observe that the typical time that NEST can sustain without heating was mostly around 1 hour. Occasionally, this duration went up to 2 hours due to lower thermal demand.

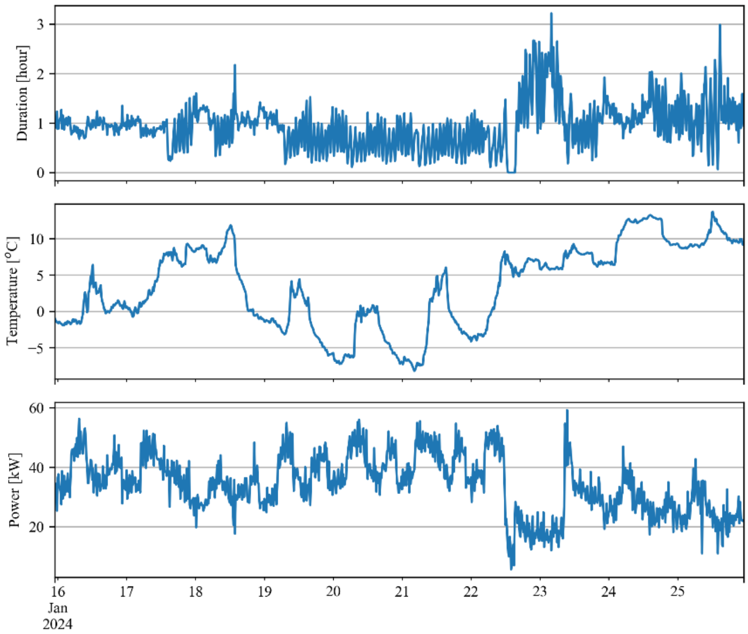


Figure 25. Flexibility from the perspective of the existing ripple control infrastructure. Top: the duration that NEST medium temperature grid can be virtually disconnected. Medium: ambient temperature. Bottom: thermal load measurements.

### 3.3.2 Modeling ehub of K3

A simplified view of the ehub at K3 is illustrated in Figure 26, including a HP, a CHP, a water buffer tank, and heat exchangers (the secondary sides of the heat exchanger are connected with the SH system and DHW system. Operation of the ehub needed to ensure that the supply side of the heat exchanger connecting heating group was above the values defined by the heating curve. The main flexibility of the ehub originates from the thermal inertia of the water tank and water within the pipes. Although the large thermal inertia of the building envelope may be another source of flexibility, it cannot be exploited in this project due to the lack of sensors and actuators in individual rooms.

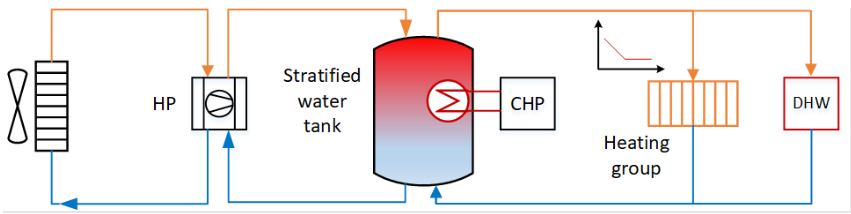


Figure 26. Simplified overview of the ehub at K3.

To exploit the thermal inertia of the water tank, we first considered tank stratification and divided the tank into four different layers (denoted as Top: top layer; Mid-top: middle to top layer; Mid-bot: middle to bottom; and Bot: bottom layer) as shown in Figure 27. We can observe the temperature difference between measurements, and the simulation over one month mainly was bounded within 4° Celsius for all layers of the tank.

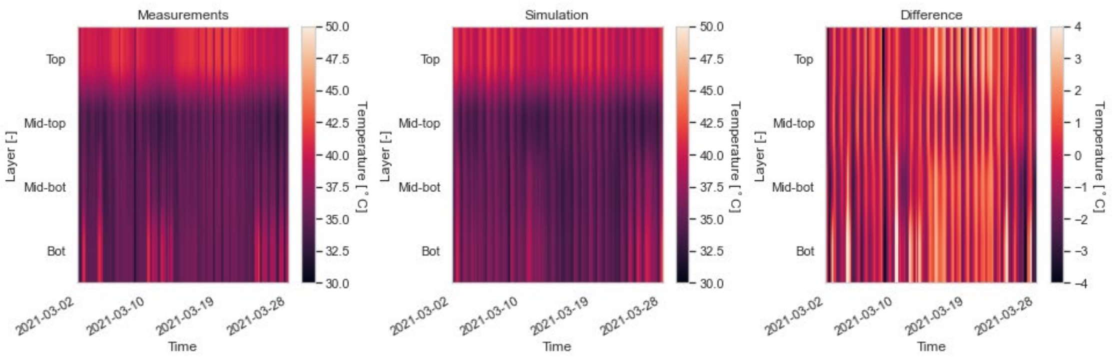


Figure 27. Simulation over one month. Left: measured water temperature at different heights of the tank. Middle: simulated temperature evolution over one month. Right: the difference between measured and simulated temperatures (note that this plot has a different scale from the other two).

We further analyzed the model accuracy in Figure 28 and Figure 29. Figure 28 shows the error of temperature modeling at different layers of the tank for different lead times. Both RMSE and mean error (ME) are presented. We can observe that RMSE for bottom, middle-bottom, and middle-top layers was around 1 degree. Figure 29 gives a concrete view of modeling errors between measurements and models.

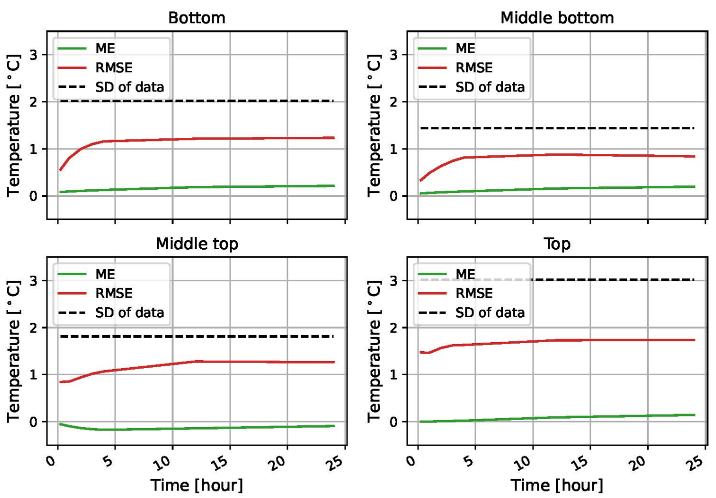


Figure 28. Summary of modeling errors of each layer with respect to various lead time.

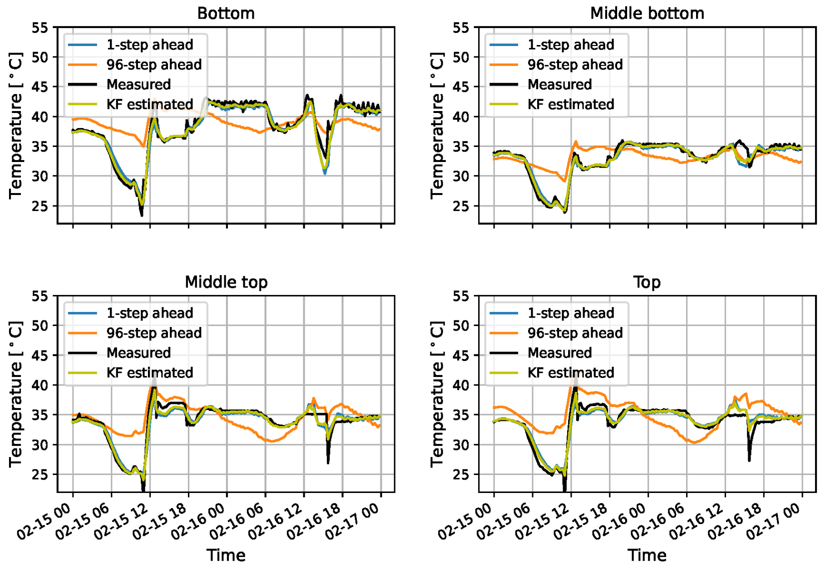


Figure 29. Model validation by comparing measurements with prediction made 1-step and 96-step ahead. Kalman filter was also implemented to estimate hidden states.

Apart from the tanks, conversion units were also modeled. For the HP, we considered a HP with part load operation, and we model its thermal output as a linear function of source and sink temperature and electrical power input. For the CHP, we consider ON/OFF operation with a constant energy efficiency and a constant heat-to-power ratio. The model of ehub was further used in the controller design and flexibility identification. We provide two flexibility analyses. The first analysis concerns a comprehensive flexibility quantification using the flexibility envelope concept (developed and experimentally implemented in previous work, e.g.(Cai and Heer, 2021)). In the second analysis, we interpret the flexibility from the perspective of the existing ripple control infrastructure, namely, how long system operators can achieve load reduction without compromising occupants' comfort.

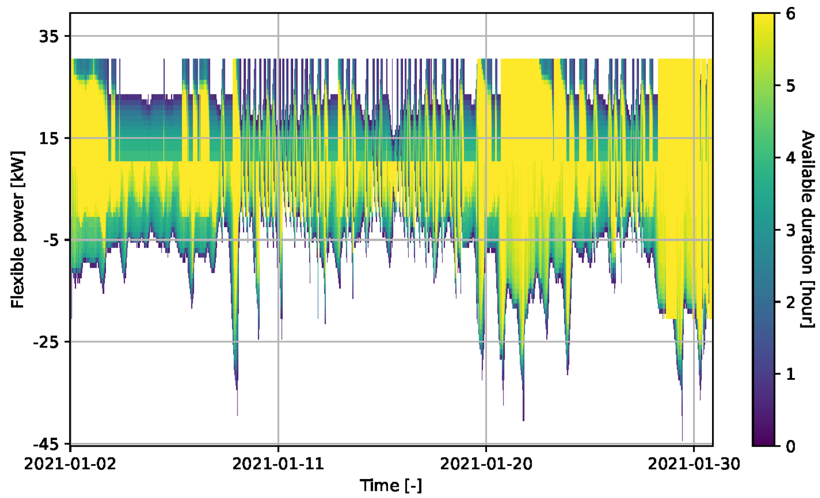


Figure 30. Flexibility envelope quantified over one month. Components included are the HP, the CHP, and the PV installation.

We can observe time-varying flexibility levels with high variance. This time dependency is highly related to weather conditions. This flexibility envelope characterized the feasible power levels (for the combination of HP, CHP, and PV) and maximally sustained duration. Energetic flexibility can be obtained when combining both. The implication of the existing ripple control infrastructure is shown in Figure 31. It can be observed that the ambient temperature substantially impacted the heating loads, affecting the duration that the load can be reduced.

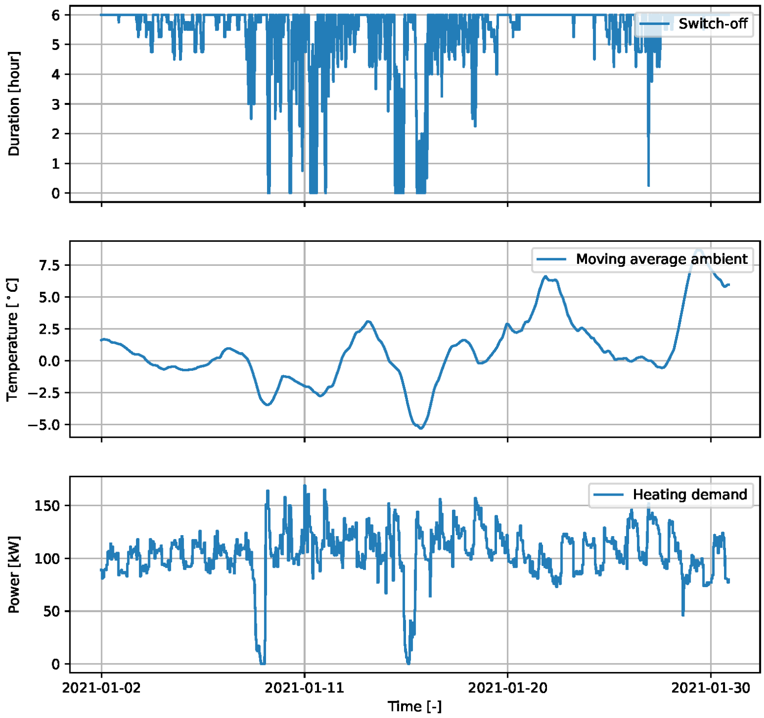


Figure 31. Interpretation of flexibility from the perspective of the existing ripple control infrastructure. Top: the duration that K3 can be virtually disconnected from the grid (I.e., the combined power of the HP, the CHP, and the PV installation is 0). Middle: moving average of ambient temperature. Bottom: measured heating load.

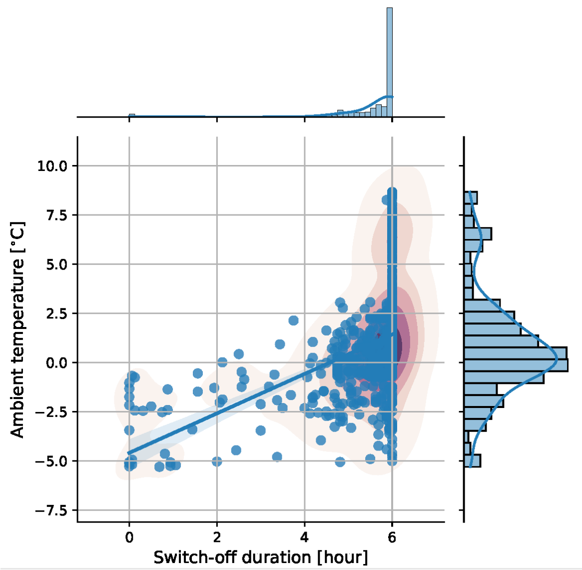


Figure 32. Correlation between the switch-off duration and ambient temperature as well as their distributions.

A linear regression analysis is provided in Figure 32 to illustrate their correlation further. It can be observed that a positive correlation exists between switch-off duration and ambient temperature. This analysis is in close analogy to heating-degree-days, which quantifies energy demand for building heating needs concerning daily average ambient temperature. Therefore, such an analysis may provide an intuitive tool to exploit flexibility based on weather forecasts (instead of the current schedule-based ripple control scheme).

### 3.3.3 Emission-aware operation: MPC vs. benchmark controller at K3

Different objective functions were evaluated and compared with the state-of-the-art rule-based operation in simulation. The results in this chapter showed how operational optimization could influence local control and, thus, the local facility and how the conventional rule-based operation performed compared with an emission-aware operation and a cost-aware operation. During the project, NEST served as a testbed for controller development before deployment at K3, and a comprehensive sensitivity analysis similar to the one conducted for K3 was not performed.

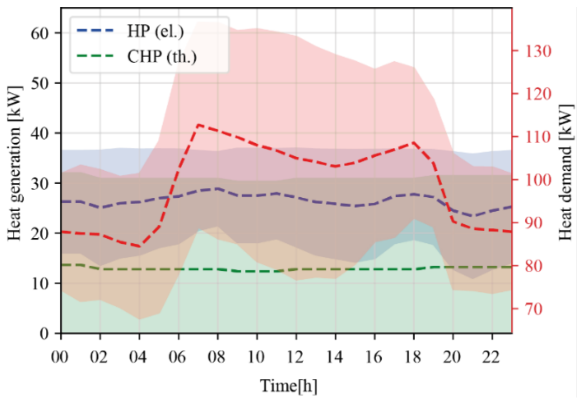


Figure 33. HP and CHP operation with the rule-based controller. Left axis indicates the heat generation of the HP and CHP, and the right axis indicates the heat demand. Dashed lines: mean. Shaded areas: mean ± 1 standard deviation.

Figure 33 shows the operation of HP and CHP for rule-based operation, together with the heat demand. Note that the HP is presented with electrical power, as the thermal power was not directly modeled in our data-driven model. However, thermal power can be derived in ex-post analysis since electrical power was highly correlated with the thermal output through COP. Therefore, the presented profile can reveal the operational pattern.

Figure 33 shows that the HP, especially the CHP, mainly operated independently of time without considering upcoming boundary conditions, such as PV electricity output. The traditional control of the K3 building's heating system, as is standard today, was based on predefined rules. To ensure that the required energy for maintaining room comfort and hot water supply is always available, the HP and CHP operated so that the temperature in the heat storage remained above a minimum level. The temperature limit in the heat storage depended on a predefined heating curve as a function of average outdoor temperature. On freezing days, when the heat demand was high, the biogas-powered CHP was activated for peak loads. The ratio of generated thermal and electrical energy was 2:1.

At K3, local PV electricity can provide cheaper and low-carbon-footprint power for HP operation than if it were drawn from the grid. It was possible to operate the different system components (HP & CHP) more efficiently through operational optimization. Common optimization objectives include minimizing energy consumption. Since the carbon footprint of grid electricity fluctuated daily, the time-adapted flexible operation could enhance sustainability. The graphs in Figure 34 show the emissions-aware operation of the HP and CHP with the heat demand (red), the carbon footprint of grid electricity (purple), and the generated PV electricity (orange).

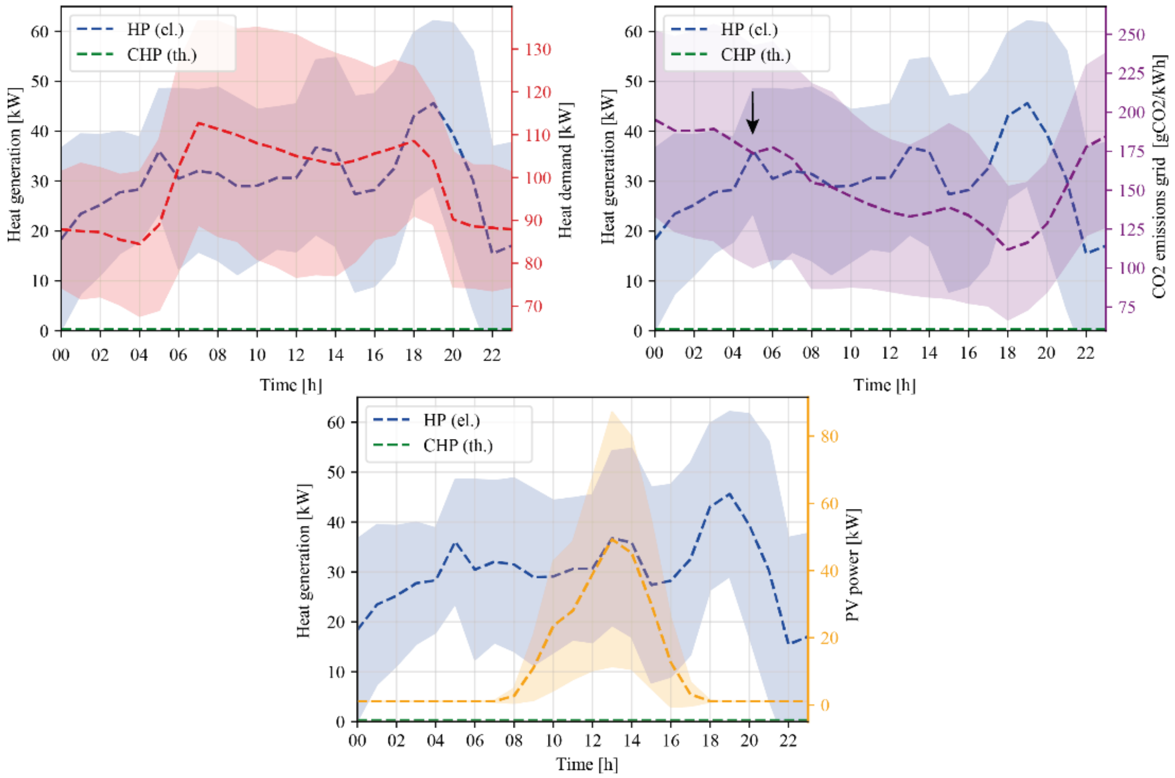


Figure 34. Visualization of operational patterns of HP and CHP in emission-aware operation. Dashed lines: mean. Shaded areas: mean ± 1 standard deviation.

The results indicated the operation of the HP was adapted to the carbon footprint of the grid electricity and the availability of clean PV electricity, which was not entirely emission-free. The embodied emissions were included with a constant carbon footprint of 50gCO2/kWh. Because the carbon footprint just before the rise in heat demand was slightly lower (indicated by the arrow), the heat storage was charged with cleaner electricity (a small HP power peak) so that shortly afterward, when the heat demand and carbon footprint rose, this heat can be released. On the other hand, the CHP was not activated during the entire heating period. The reason is the high carbon footprints of the gas compared with the varying grid electricity. The emissions for thermal energy from the HP corresponded to the grid electricity carbon footprint, divided by the HP's Coefficient Of Performance (COP). With an average COP of 3, a carbon footprint of 13 - 139gCO2/kWh (min, max) can be expected for the HP. The carbon footprint of biogas was higher at 215gCO2/kWh. The impacts of the carbon footprint of (bio-)gas will be presented later in this chapter.

The cost-optimal operation was also examined, where the controller guarantees heating operation at minimal operating costs. In Figure 35, the HP and CHP operations are depicted again with the heat demand (red) and newly the grid tariff (purple). The results showed how the operating times of the HP were adapted to the grid electricity costs, and the low-tariff phases in the morning were exploited. The heat storage was charged early in the morning at favorable conditions. This heat surplus could then be redistributed to the building when the heat demand and electricity tariffs increased. Compared with the emission-aware operation, the cost-aware operation showed no increased utilization of PV electricity.

The reason is the high grid feed-in tariffs of 18.95 Rp/kWh[10]. The CHP was again not used because the gas price of 15.3 Rp/kWh[11] was too high compared to the heat-equivalent electricity price (grid tariff & COP) of the HP.

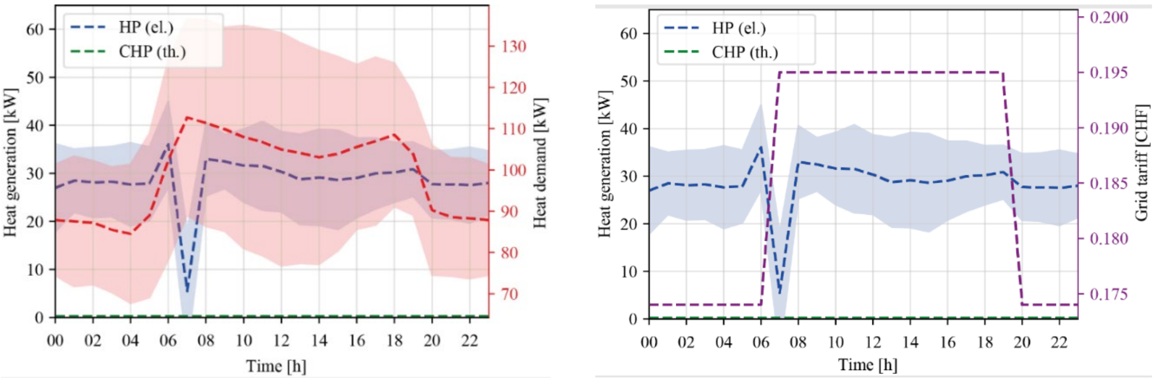


Figure 35. Simulation results of cost-optimal operation. Dashed lines: mean. Shaded areas: mean ± 1 standard deviation.

All three previously discussed controllers were compared in simulation for one year. The percentage deviation from the rule-based controller was also listed for both MPC controllers. The results summarized in Table 4 were aligned with expectations that the emission-optimal MPC would significantly reduce carbon footprint and the costs-optimal MPC would reduce costs (total costs including peak load costs). In all cases, the heat demand to be met was identical. Due to the lack of heat from the CHP, additional electricity from the grid must be imported for HP operation.

Table 4. Comparison between rule-based controllers and MPC controllers minimizing emission and cost.

| Indicator | Rule-based | Emission-MPC | Cost-MPC |
|---|---|---|---|
| HP (el.)/CHP(th.) [MWh] | 124.5/29.0 | 135.8 / 0.0 (+9% / -100%) | 125.8 / 0.0 (+1% / -100%) |
| Imported el. Energy [MWh] | 239.4 | 258.0 (+8%) | 255.2 (+7%) |
| Exported el. Energy [MWh] | 143.8 | 136.6 (-5%) | 143.8 (0%) |
| Emissions [tCO2] | 42 | 33.5 (-20%) | 35.0 (-17%) |
| Cost [kCHF] | 78.4 | 76.3 (-3%) | 74.2 (-5%) |
| Peak Load Cost [kCHF] | 13.7 | 15.3 (+12%) | 13.2 (-4%) |

Figure 36 provides a detailed analysis of heating periods throughout the year, comparing results for all four seasons using indicators from Table 4.

[10] die werke AG, Strompreislisten 2022; https://www.diewerke.ch/preislisten-strom
[11] die werke AG, Gaspreislisten 2022; https://www.diewerke.ch/gaspreise

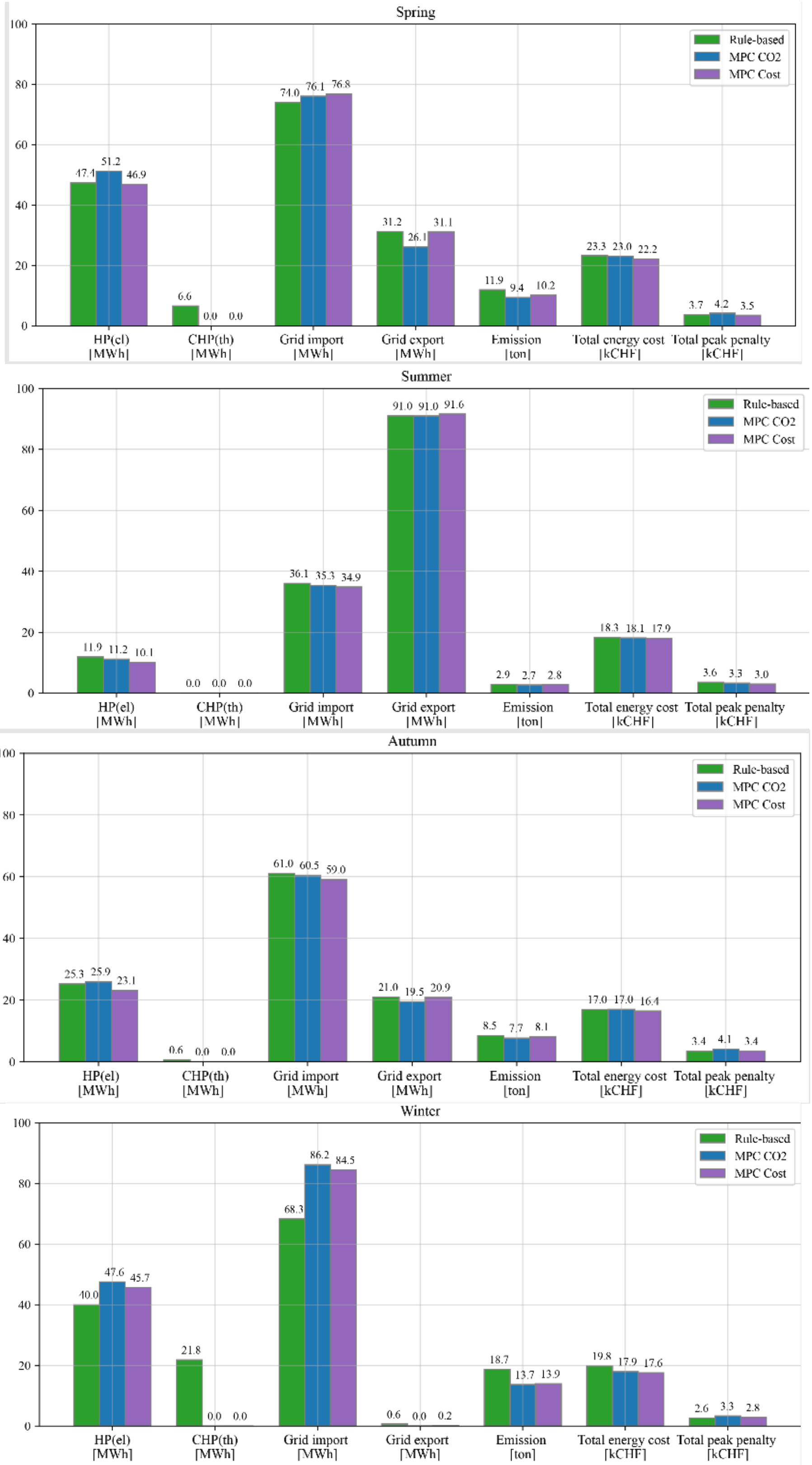


Figure 36. Comparison across different seasons.

Both MPC controllers demonstrated significant cost and emission savings during winter when the HP operated most frequently. Increased HP usage in winter led to higher electricity imports and zero exports. Installation of PV facades allowed for additional electricity generation in winter, aiding emission-aware operation due to reduced carbon footprint. Despite a high proportion of PV electricity in summer, savings potential was limited. The PV system generated surplus power midday, necessitating direct export as storage was currently unavailable. Integration of a battery could facilitate the evening reuse of clean electricity, promoting sustainability.

Furthermore, HP electricity demand for summer cooling was notably lower than for winter heating, resulting in smaller optimization potential mainly from HP operation. Significant summer savings came from reduced peak load costs. Transitional spring and autumn periods offered moderate savings potential in both costs and emissions.

In the operational optimization results, the significant HP capacity relative to the heat demand, alongside the lower carbon footprint of grid electricity compared to gas, suggested that the CHP system was not necessary year-round. This prompts the question: at what level of gas carbon footprint does utilizing the CHP become viable?

Figure 37 shows the influence of the gas carbon footprint on the use of the CHP and the total emissions of the overall system for the winter months for an emission-aware controller and the rule-based control. The results indicated that as the CO2 penalty decreased, the operating hours would increase, and emissions would decrease. If the gas footprint dropped below 160gCO2/kWh, the emissions-optimal controller in K3 would increasingly operate the CHP instead of the HP. Further, at a gas footprint below 95gCO2/kWh, the CHP, designed to cover peak load, would be used more than in the classic rule-based operation.

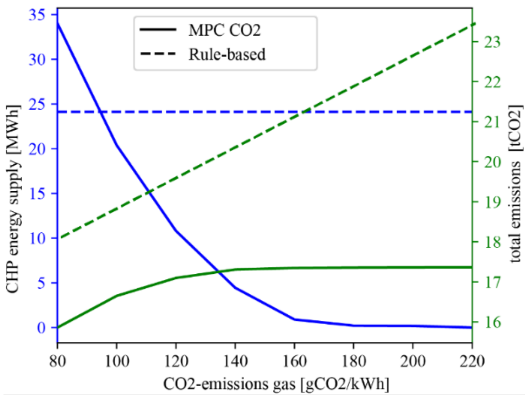


Figure 37. Correlation between CHP operation and CO2 emissions from gas input.

### 3.3.4 Experimental results on emission-aware operation at NEST

The experiments at NEST were conducted in two configurations: energy hub with PV and energy hub with PV and battery. Figure 38 summarizes measurements from the benchmark year and closed-loop control experiments at NEST, with and without a battery, showcasing daily GWP, thermal power input to the energy hub, and PV output. We can observe that GWP values were consistently higher in the benchmark case. Thermal power output exhibited increased fluctuations in the controlled cases, but this did not directly correspond to the GWP pattern because the emission-aware optimization aimed to minimize the overall carbon footprint, including both electricity import and embodied emissions from self-consumed PV output for all the components.

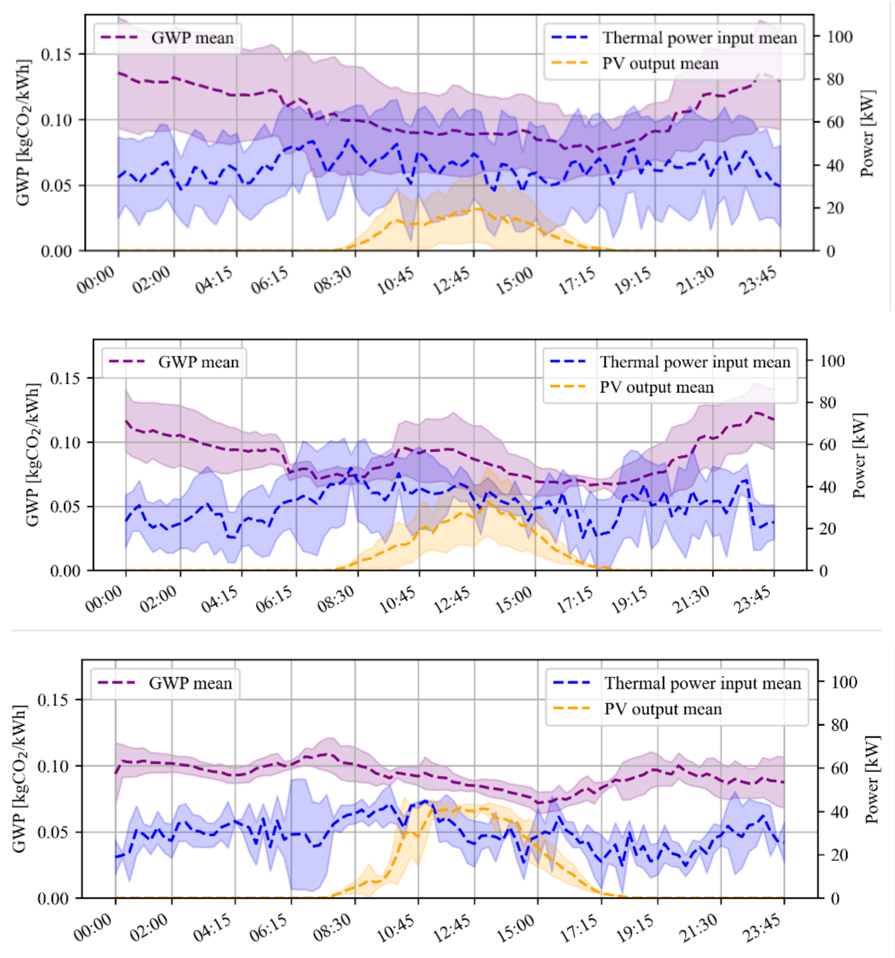


Figure 38. The daily patterns of GWP and thermal power input to the energy hub. Top: benchmark results. Middle: results from a closed-loop control experiment without a battery. Bottom: results from a closed-loop control experiment with battery. Dashed lines represent the mean values, and the shaded areas indicate one standard deviation range from the mean.

The above observation prompts us to analyze the net import at NEST, as shown in Figure 39, where the reference case had more electricity import than the controlled case in general. The imports during midday were particularly high due to different PV outputs. The net import exploited the lower GWP values during the early morning in the controlled cases. In all cases, the net import was lower during nighttime when GWP peaked.

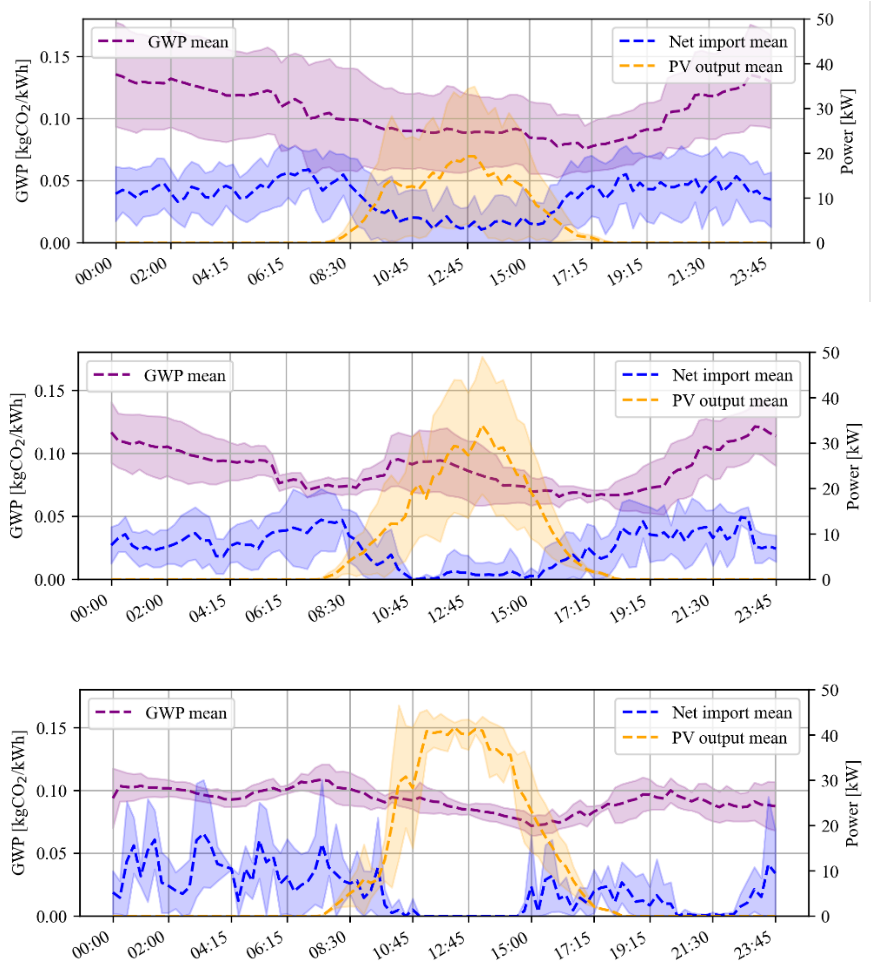


Figure 39. The daily patterns of GWP and net electricity imports from the grid. Top: benchmark results. Middle: results from a closed-loop control experiment without a battery. Bottom: results from a closed-loop control experiment with battery. Dashed lines represent the mean values, and the shaded areas indicate one standard deviation range from the mean.

The average tank temperature daily patterns in both cases are shown in Figure 40, where the emission-aware controller regulated the temperature, adapting to the patterns of GWP. It can be observed that electricity imports during the middle of the day were significantly reduced in the control case compared to the benchmark case. This reduction is attributed to storing heat in water tanks, effectively decreasing the need for electricity imports during peak hours.

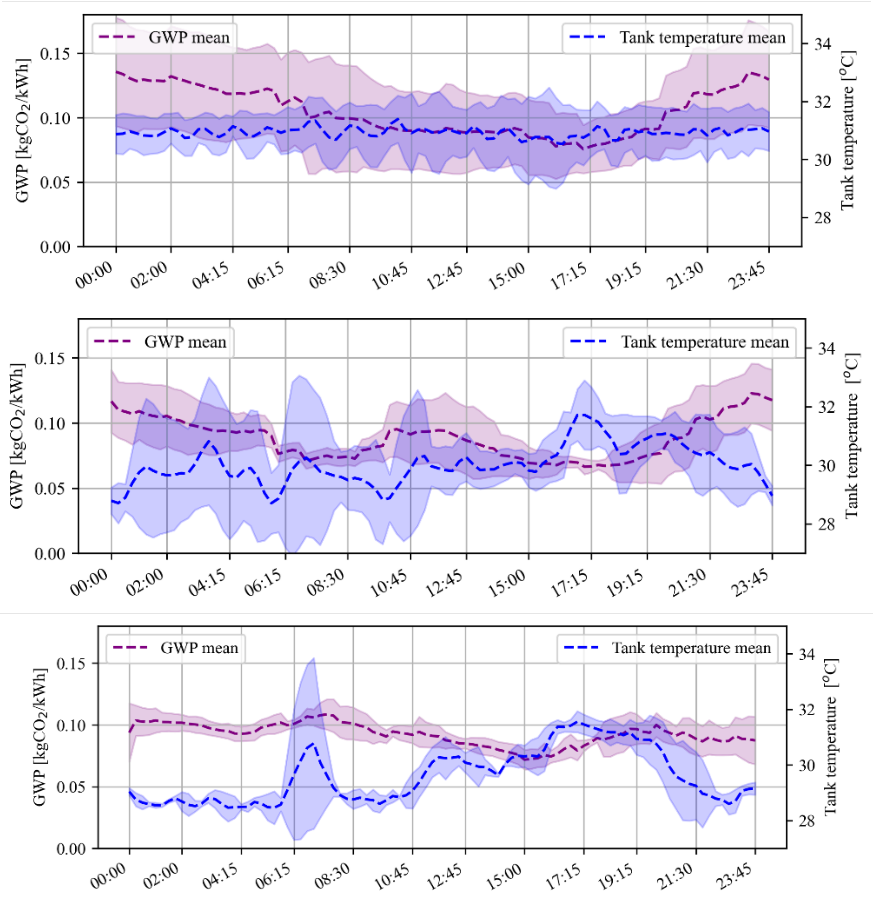


Figure 40. The daily patterns of GWP and buffer tank temperature. Top: benchmark results. Middle: results from a closed-loop control experiment without a battery. Bottom: results from a closed-loop control experiment with battery. Dashed lines represent the mean values, and the shaded areas indicate one standard deviation range from the mean.

Next to the time series view in previous figures, Statistics of daily carbon footprint given different mean daily ambient temperatures are summarized in Figure 41. Generally, as the daily ambient temperature increased, the daily total carbon footprint decreased. This was due to higher heating demand during cold weather. Additionally, the y-intercepts of the controlled cases were lower, indicating a lower carbon intensity across all temperatures than the benchmark, particularly effective at lower ambient temperatures.

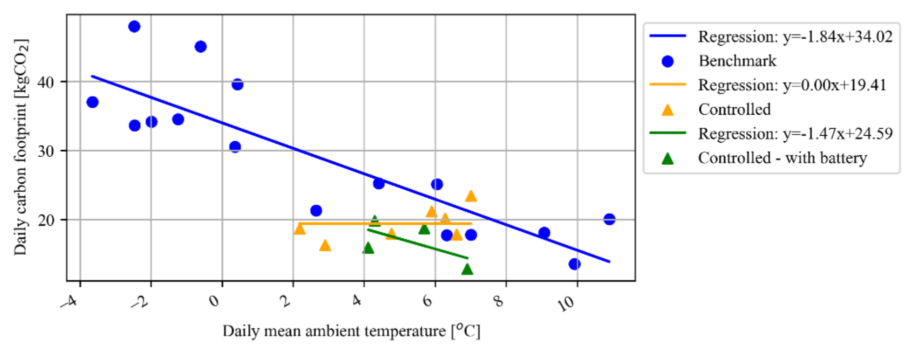


Figure 41. Daily carbon footprint given different mean daily ambient temperature. The colors differentiate the benchmark case from the two control cases.

However, the GWP values were different across these cases. Therefore, the GWP values during these periods were further shown in Figure 42 to contextualize the numbers, with additional regression analyses revealing relations between average carbon footprint and daily mean ambient temperature. As shown in previous figures, the GWP values were lower in the controlled case than in the benchmark case. Additionally, part of the reduction in carbon footprint can be attributed to the PV output; therefore, we further normalize the average footprint by dividing the realized carbon footprint by the calculated GWP values, as the statistics shown in Figure 43.

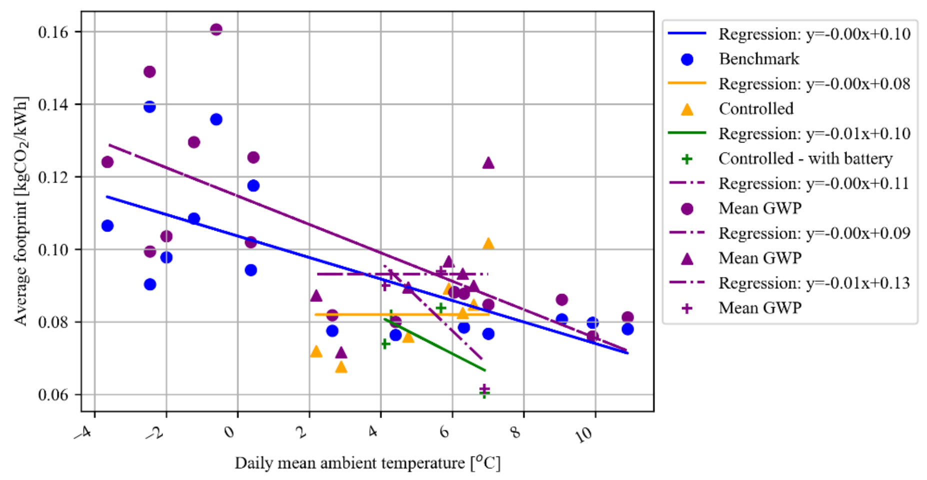


Figure 42. Daily average carbon footprint given different mean daily ambient temperature.

The range of values (as indicated by the whiskers of the boxplot) appeared more significant in the benchmark case than in the controlled cases. This could suggest that the controlled cases reduced the average carbon footprint compared to the benchmark case. In the benchmark case, the normalized footprints had a median of 94%. This indicated that installing PV systems contributed to a 6% reduction in the normalized average carbon footprint. In the controlled case without a battery, the median normalized value is 88%, suggesting a combined contribution from PV outputs and load shifting. Consequently, the additional reduction attributable to load shifting was calculated to be 6%. In such cases, the impacts of PV installation equaled load shifting in reducing carbon footprint. When a battery was added, the median normalized value was 89%, and the spread was narrower than the case without a battery, suggesting that a battery of the specific energy capacity did not provide additional reduction benefits, but the consistency of the footprint reduction may have been improved.

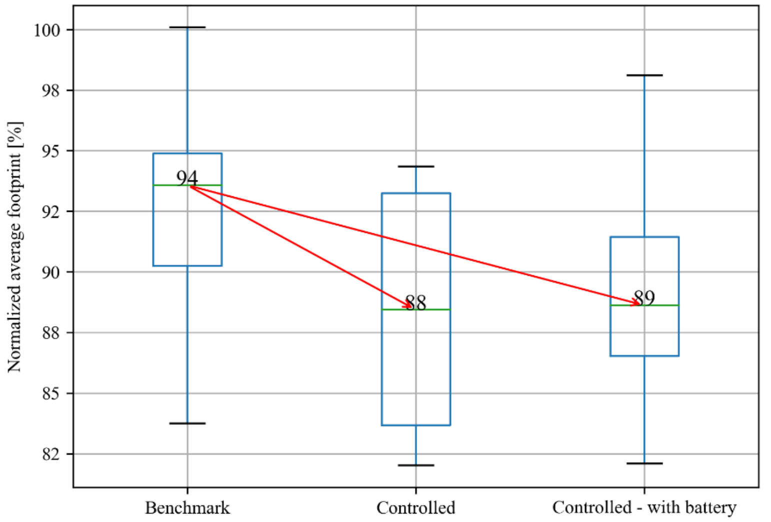


Figure 43. Average daily carbon footprint normalized by GWP values in the benchmark and controlled results with and without battery.

### 3.3.5 Experimental results on emission-aware operation at K3

The daily trends in GWP, the electric power input of the heat pump, and the output of CHP are shown in Figure 44. It also includes Pearson correlation coefficients for the power input of heat pumps against GWP values. In both cases, CHP power was at minimal levels. It can be observed that the GWP was, on average, higher in the benchmark case than in the controlled case. Additionally, the carbon footprint exhibited more significant variability in the benchmark case (i.e., in 2022) than in the controlled case. In both cases, the heat pump's electric power input was higher during the day than at night. The Pearson correlation coefficients were negative in both cases, revealing the opposite trend and potentially indicating HP consumption at low GWP values.

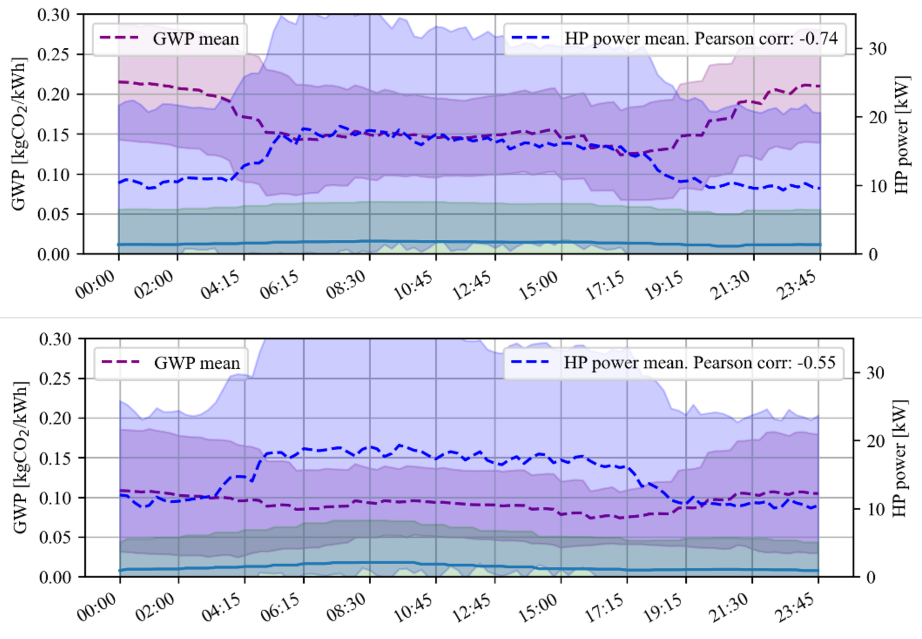


Figure 44. The daily patterns of GWP and HP electrical power. Top: benchmark results. Bottom: results from a closed-loop control experiment. Dashed lines represent the mean values, and the shaded areas indicate one standard deviation range from the mean.

The daily patterns of GWP alongside PV output are presented in Figure 45. Note that onsite PV was sporadically in partial operation in the benchmark case. Therefore, synthesized PV output based on solar irradiance, which surpassed actual field measurements, is presented.

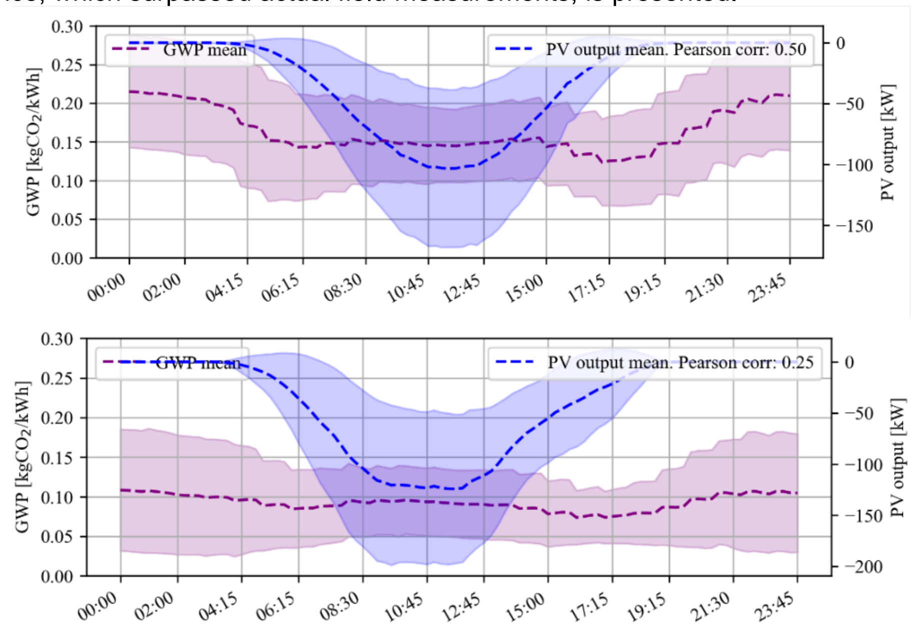


Figure 45. The daily patterns of GWP and PV output. Top: benchmark results. Bottom: results from a closed-loop control experiment. Dashed lines represent the mean values, and the shaded areas indicate one standard deviation range from the mean.

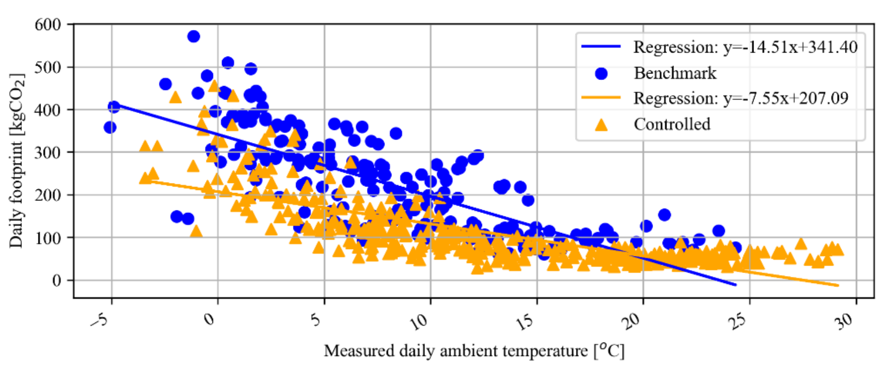


Figure 46. Daily carbon footprint at different average daily ambient temperatures.

Figure 46 demonstrates the relationship between average daily ambient temperatures and the daily carbon footprint, with regression analyses for benchmark and controlled cases. A negative correlation indicated that the total daily carbon footprint increased as temperatures decreased. Notably, the daily carbon footprint in the controlled case was consistently lower than in the benchmark case, potentially suggesting carbon footprint reduction has been achieved. The total carbon footprint in the benchmark case was 46.5tCO2, whereas it was 40tCO2 in the controlled case. This indicated an improvement of 14%. However, due to varying GWP profiles across the two periods, further analysis was needed to quantify this improvement, as shown in Figure 47, where the daily average carbon footprint was shown together with daily ambient temperatures. Additionally, the daily average of GWP values were presented. In both benchmark and controlled cases, the average carbon footprint was lower than the daily average of GWP values. This phenomenon was attributed to PV output, which an embodied emission of 50gCO2 per kWh has been assumed.

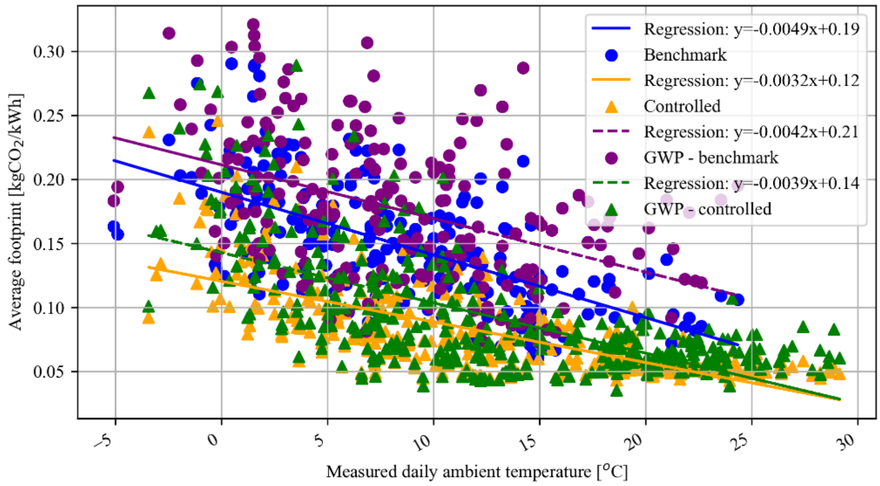


Figure 47. Average carbon footprint per kWh of energy consumption (including both thermal and non-controlled electrical loads) at different average daily ambient temperatures.

Comparative regression analysis reveals that the regression slope decreased relative to the real GWP in the controlled case. In contrast, the regression slope increased in the benchmark case, indicating that the control measures implemented in the experiments reduced the carbon footprint against the benchmark.

To isolate the impacts of different GWP values in the different periods, the average carbon footprint was further normalized using the GWP values, and the statistics are presented in Figure 48. The boxplot suggested that PV potentially reduced the average carbon footprint by 11% in the benchmark case. The total carbon footprint was reduced by 12% in the controlled case. Although Figure 47 indicated a reduction in carbon footprint of 14%, the normalization process revealed that the normalized difference is not substantial. In comparison, the results summarized in Table 4 for the simulation-based study showed an ideal carbon footprint reduction of 20%. We can observe a gap between simulation and practical realization.

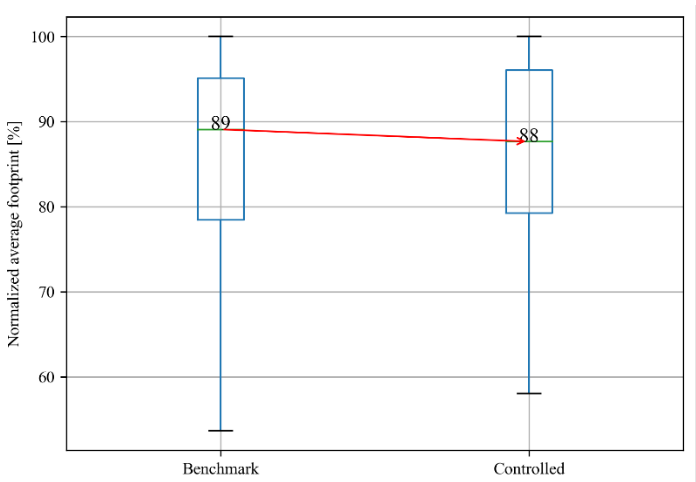


Figure 48. Boxplot of average carbon footprint normalized by the GWP values.

Several factors and practical challenges potentially contributed to this gap:

1. It is important to acknowledge that simulation-based performance comparisons evaluated different controllers under identical model and boundary conditions from the same period. In contrast, experimental performance comparisons lacked a universal comparison method. The report compared performance gains with a reference year when a different controller was implemented, with different boundary conditions and load profiles. Therefore, the performance gains were not directly comparable.
2. This project mainly considered thermal demand flexibility. However, the analysis in sub-chapter 3.3 showed a relatively minor share of thermal demand in overall energy consumption. This impacted the contribution of thermal load shifting to reduce carbon footprint at the building level.
3. The actuation capabilities of the infrastructure were significantly different from the expected actuation. More specifically, there was consistent under-actuation when sending the control set points. The interface implementation team did not resolve such ad-hoc technical challenges during the project.
4. Due to the data quality issue, a large spread of GWP values strongly impacted the forecast performance of GWP. The variations were not static, as shown in sub-chapter 3.1.
5. The GWP profile in the controlled case had significantly less variances on average. This led to lower carbon footprint reduction potentials through load shifting.
6. Sporadic interruptions (such as the communication server being down over the summer, the HP/CHP being down) also contributed to the gap.

Comparing the results from NEST and K3, we can observe that predictive control has the potential to reduce carbon footprint. However, the practical implementation still faces several hurdles. These include establishing a stable and universally accepted carbon footprint profile, standardizing processes for efficient and reliable hardware and interface implementation, ensuring dependable system integration, balancing control performance with the need to access external information sources, and developing an intuitive and transparent methodology for performance quantification towards trust and acceptance.

## 3.4 Experimental results on data-driven predictive control

This part of the results has been derived using the method in Chapter 2.5. Since this method was developed late, it was impossible to integrate it into the intended measurement campaign on carbon-aware operation. Instead, a few simulation and experimental case studies have been carried out to prove the efficacy of the proposed method. These experiments have considered common objectives of DSM, such as tracking reference signals from system operators and energy consumption minimization. The algorithms have been extensively assessed according to DSM tasks. More specifically, various platforms have evaluated different common controlled systems within the residential sector and common DSM control tasks. This is summarized in Figure 49.

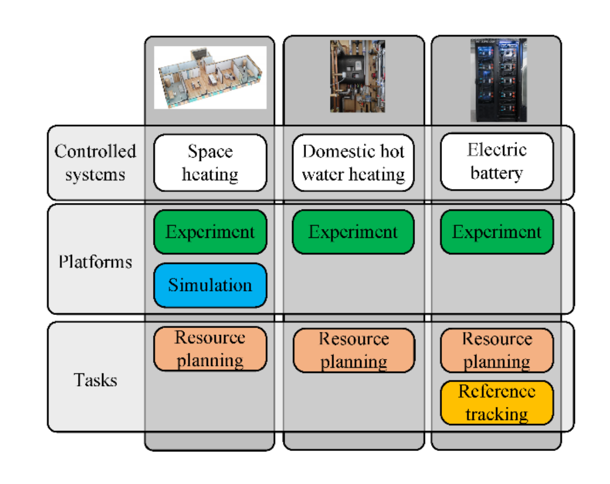


Figure 49. Summary of the investigated experimental case studies at NEST (Yin et al., 2024)

In the rest of this report, only the experimental results are selected to be summarized in Figure 51, and Figure 52, for control tasks on space heating, domestic hot water heating, and stationary battery. Simulation results can be found in (Yin et al., 2024).

The experimental results revealed that the SMM-PC algorithm performed well regarding constraint satisfaction, and its performance can be transferred to different types of systems with minimal tuning effort. Therefore, the SMM-PC algorithm can potentially enable large-scale deployment of DSM across heterogeneous systems in a timely manner.

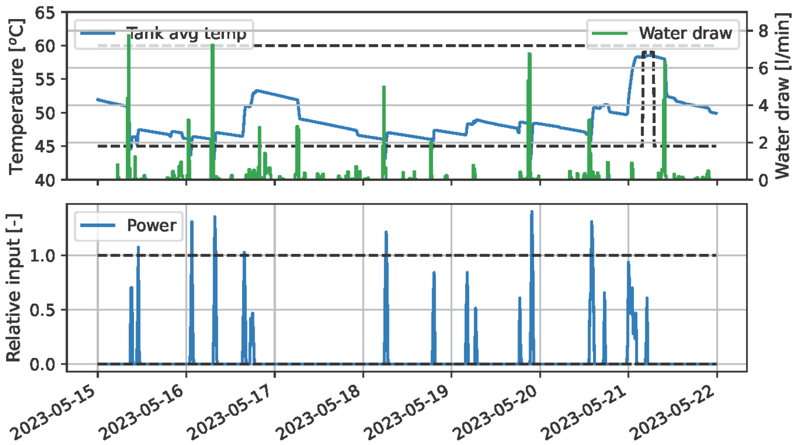


Figure 50. Experimental results of controlling domestic hot water heating. Top plot: the solid blue curve shows the average tank temperature trajectory, and the dashed black lines indicate temperature limits (scale at left). The solid green curve shows the actual water draw profile (scale at right). Bottom plot: the solid blue curve shows the measured thermal power into the tank and the dashed black lines indicate expected thermal power limits. The maximum power varies depending on supply temperature.

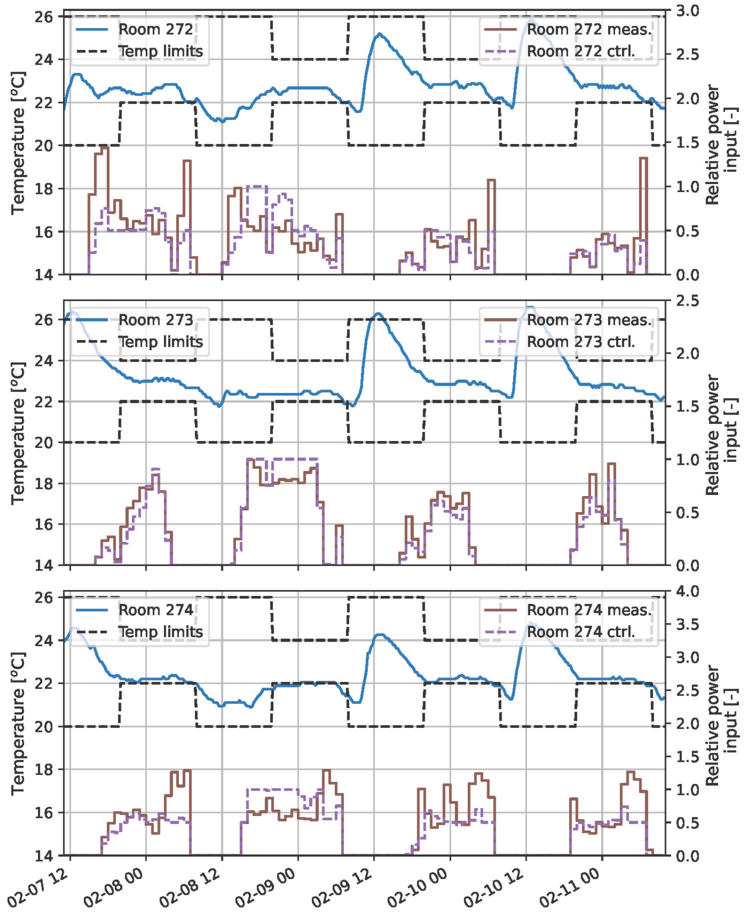


Figure 51. Experimental results of space heating control. Top plot: results for Room 272. Middle plot: results for Room 273. Bottom plot: results for Room 274. The dashed black curves show temperature limits. The solid blue curves show temperature trajectories. The dashed purple curves show controller decisions (scale at left). The solid olive curves show realized thermal power inputs into the rooms in relative terms by normalizing using thermal power capacities (scale at right).

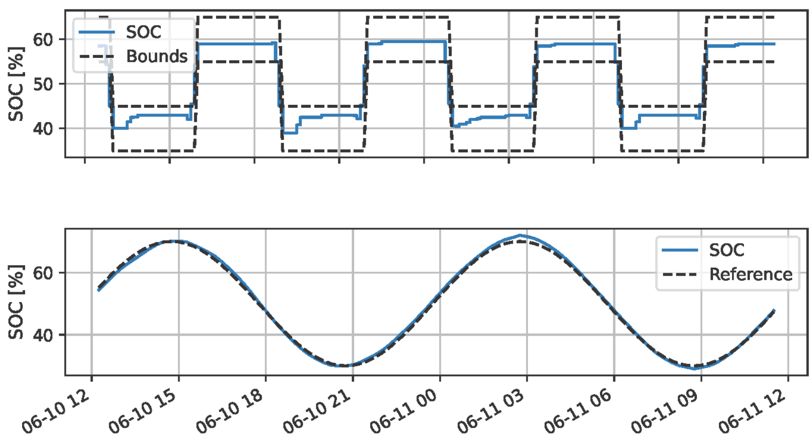


Figure 52. Experimental results for the control of an electric battery. Top plot: resource planning task. Bottom plot: reference tracking task. The solid blue curves show the actual SOC. The dashed black lines indicate temperature limits for the top plot and the reference trajectory for the bottom plot.

Two main observations can be drawn from the quantitative results. Firstly, compared to the state-of-the-art data-driven predictive control algorithms, the proposed algorithm can improve occupants' thermal comfort and energy saving by up to 90% and 8%, respectively. This assessment was made in simulation using the high-fidelity model presented in (Fazel Khayatian et al., 2022). More details on the benchmark algorithms and comparison can be found in (Yin et al., 2024). Secondly, the algorithm effectively ensures constraint satisfaction, and its performance can be transferred to other systems with minimal tuning effort. Therefore, the proposed algorithm can facilitate large-scale deployment of demand-side management to support energy system operation.

Lastly, even though the methodology is only rigorously proven for linear systems, this work's numerical and experimental studies show that it can be effectively applied to nonlinear systems by considering nonlinearity as an additional source of error, with better performance than conventional algorithms based on linear system identification.

## 3.5 Space heating demand flexibility at the national scale

This part of the results is related to the method documented in Chapter 2.6. Example results are shown in Figure 53. National-scale space heating demand flexibility was normalized and expressed as the duration for virtual disconnection, derived from the flexibility envelope concept outlined in Chapter 2.4. Virtual disconnection resembles the DSO approach, where a ripple control signal is sent to disconnect the load from the grid. Although average values aligned with Swiss climate conditions, absolute values were influenced by the number of buildings within each commune, revealing significant regional disparities across Switzerland. When planning energy infrastructure considering energy flexibility, such disparity may need to be included.

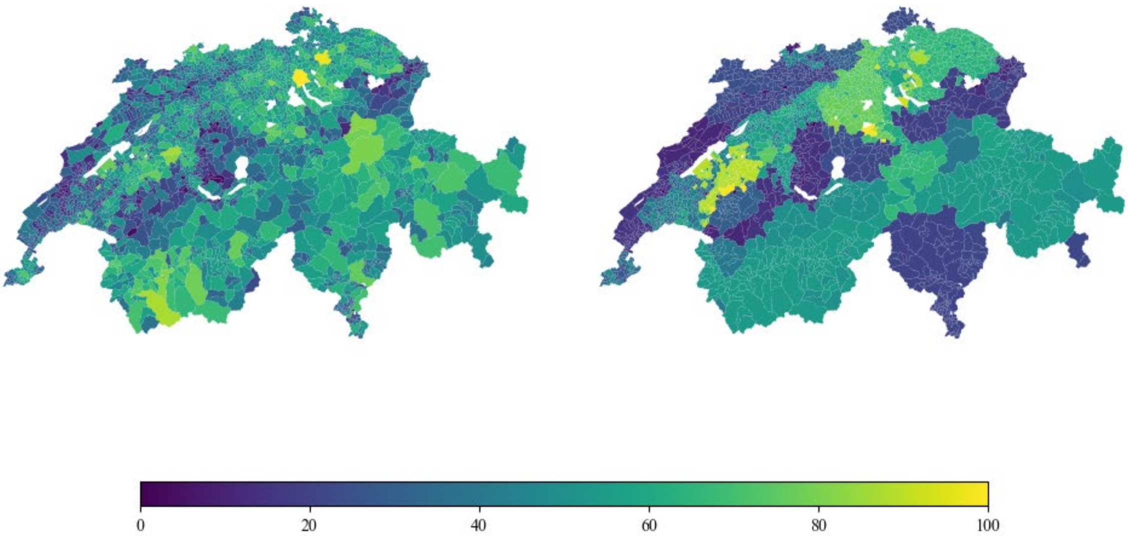


Figure 53. Normalized space heating demand flexibility at a national scale, representing the duration for virtual disconnection. Left: aggregated flexibility within each commune. Right: average flexibility within each commune.

# 4 Conclusions

In this project, our contributions to demand-side management (DSM) have centered on minimizing the carbon footprint (CF) of electricity consumption in buildings using optimization-based methods. We developed a forecasting tool for the definition of short-term average CF profiles of the Swiss electricity mix that utilizes public datasets, which provides a critical tool for enabling emission-aware DSM. Offline training results with historical CF profiles suggest that linear regressors can achieve satisfactory forecasting accuracy when utilizing the electricity statistics of the rolling two-month period as an input parameter. Indeed, our comprehensive analysis of performance from other more complex machine learning models did not yield substantial additional advantages. However, in real-time forecasting, we encountered difficulties in consistently obtaining high-quality public datasets for the rolling two-month period, especially from the ENTSO-E platform, which created unforeseen issues in completeness and quality of our forecasting that was done for more than a year.  This issue has not been resolved within the project's duration since it will probably require collaboration with organizations that are the providers of electricity statistics. Potential future research and enhancement directions could be found here.

Our research has also compared predictive control operations with traditional rule-based controllers. At NEST, experimental findings show that load shifting and PV installation have equally contributed to a 12% reduction in the average CF of the building when compared to the raw CF values of the building without control measures. However, additional battery storage of the chosen capacity did not result in further reduction despite a more concentrated spread of normalized CF. At the K3 building, simulation results indicate a 20% CF reduction potential when comparing rule-based and predictive controllers under identical model and boundary conditions from the same period. The experimental findings show a 14% decrease in total CF during 2023 experiments compared to reference measurements in 2022 with CF values that were generally lower during the experiments. After normalization using CF values, a marginal improvement in reducing the normalized average CF was observed. Discrepancies between simulation and experiments can be attributed to forecasting inaccuracies, system modeling limitations, hardware actuation constraints, intermittent infrastructure disruptions, and much lower CF variance during the experiments (when compared to the CF variance of previous years). Additionally, differing methodologies for quantifying performance gains in simulation and experimentation were noted. These findings suggest that improving stakeholder involvement and integrating control solutions directly with on-site management systems could alleviate these challenges and reduce the gap between simulation and experiments.

The project also explored a novel data-driven control algorithm for DSM, showcasing its scalability and transferability. Notably, this algorithm outperforms current data-driven predictive controls by enhancing occupants' thermal comfort and energy efficiency by up to 90% and 8%, respectively. It also consistently meets operational constraints and can be applied to various systems with minimal adjustments. Therefore, the proposed algorithm addresses one technical roadblock to the large-scale deployment of DSM. Last but not least, the report offers preliminary insights into the national distribution of building space heating flexibility, exploring the variability across different building types, ages, and climatic regions. This sets the stage for future research, merging theoretical flexibility potential with practical implementation gaps, which will provide a more accurate estimation of exploitable flexibility at the system level, contributing to developing comprehensive national energy management strategies.

In conclusion, the results presented in this report describe the complexities of integrating DSM strategies into the existing systems and show the importance of addressing data quality, system integration, and scalability challenges. The findings also address several technical hurdles in achieving realistic and scalable demand-side management while highlighting key areas requiring further research and development to realize more efficient, reliable flexible, and sustainable energy systems for buildings in Switzerland.

# 5 Outlook and next steps

Four key outlooks are outlined below.

We encountered unexpected problems with the quality and completeness of recent ENTSO-E data. Highlighting these issues to appropriate stakeholders is crucial to improving our capacity to provide reliable short-term CF forecasts. One approach involves leveraging persistence forecasts using older data from the previous year. This suggestion focuses primarily on older historical data (more than two months in the past) to avoid the results being affected by recent database changes (e.g. in the last day), as it does not account for variations over time. However, the reliability of such a forecasting approach is questionable because there is an expectation that the shares of energy sources will evolve quickly in the coming years for European countries that have set ambitious GHG reduction targets. Furthermore, the existing commercial CF forecasting service has a notable transparency issue. The specific data sources utilized remain unclear, raising questions about the potential for using alternative data sources, including data from Swissgrid. While market clearing presents an alternative, it predominantly operates within a financial framework and may not accurately reflect the physical production realized. It would be interesting to start discussions with Swissgrid and the many energy providers of Switzerland to identify if other sources of information could be used to get the latest information on electricity production. Furthermore, it could be even better for our DSM approach if they agreed to share their day-ahead forecast of electricity production that we could then easily transform into a short-term forecast of the CF signal.

The project's success is closely linked to the coordination between development processes, stakeholder engagement, and the responsiveness of implementation partners. Despite the significant potential, achieving economical and scalable deployment is hampered by delays in infrastructure upgrades and the need for better coordination among diverse partners. The lack of standardized pipelines and different expectations and terminology across disciplines create substantial bottlenecks. Addressing these issues is crucial for realizing the project's full potential and is essential for scalability.

In future efforts to ensure robust estimates, it is crucial to include reliability assessments when quantifying flexibility and carbon footprint reductions. This is particularly important in complex information flow scenarios involving many external stakeholders, such as communication servers, hardware manufacturers, and interface implementation teams. Interruptions in communication and infrastructure issues can diminish performance. Preliminary research in this area has been initiated through a semester project[12] supervised by the authors of this report.

Further research is recommended to explore the sustainability of the proposed control strategies, which include sensing, actuation hardware, and computing resources. For instance, another study[13] by the lead author proposes reducing the carbon footprint by repurposing discarded electronics with sufficient computing capabilities. However, assessing the precise environmental benefits of this approach is identified as an area for future investigation.

[12] Jacquet, C., 2024. Reliability of demand-side flexibility for power system operation support. Semester Project Report, Reliability and Risk Engineering Lab, Swiss Federal Institute of Technology (ETH) Zurich.
[13].Cai, H., 2023, November. Circular economy meets building automation. In Journal of Physics: Conference Series (Vol. 2600, No. 19, p. 192011). IOP Publishing.

# 6 National and international cooperation

## 6.1 National collaboration

This project is linked to a FOGA supported project concerning analyzing energy flows in K3 and establishing the technical connectivity (bi-directional data communication) between K3 and Empa. In this context also the S-DSM project has been presented at the "3. Forschungstag der Schweizer Gaswirtschaft". An Empa internal project called "carbon footprint optimization of electricity in smart buildings (CAPITAL)" has been conducted to be able to extend the development and analysis of CF aware building control. The methods developed here in S-DSM are picked up in the SFOE SWEET PATHFNDR and serve as baseline energetic flexibility definition. The activities of Task 3.1 and Task 3.2 are conducted jointly with the NCCR Automation. Intermediate results were presented in the seminar of International Energy Agency (IEA) Annex 82 working group and received feedbacks from the international experts. Tasks related to the move demonstrator and data-driven predictive control have been investigated in collaboration with the NCCR Automation. The modeling task involves collaboration with SFOE SWEET PATHFNDR. This project is linked to a FOGA supported project concerning analyzing energy flows in K3 and establishing the technical connectivity (bi-directional data communication) between K3 and Empa. Additionally to the stated publications, an article in Aqua&Gas describing these activities and the link to SFOE via S-DSM has been published.

## 6.2 International outreach

The lead author actively participated in the International Energy Agency (IEA) Annex 82 working group throughout the project, achieving significant outreach through two main initiatives:

1) The lead author organized a two-day work meeting[14] at Empa, hosting 43 international experts to discuss building energy flexibility and its critical enablers.

2) In collaboration, the lead author co-organized a special issue with the Springer Journal, Building Simulation: An International Journal[15], titled: Energy flexible buildings for resilient low carbon built environment and energy systems.

Additionally, the lead author was invited to give a talk at the Intelligent Building Operations (IBO) Workshop in Boulder, organized by the University of Colorado Boulder. The talk covers the method and results presented in Chapter 2.5 and Chapter 3.4.

[14] https://annex82.iea-ebc.org/event?EventID=8069
[15] www.springer.com/journal/12273

# 7 Publications out of the S-DSM project

The following publications have benefited from the research work within the S-DSM project, and the project has been acknowledged explicitly.

Heer, P., Brandes, M., Cai, H. and Palla, H., 2023. K3 Handwerkcity. Der Gewerbepark erreicht hohen energetischen Selbstversorgungsgrad. *Aqua & gas*, 103(6), pp.20-26.

Cai, H., & Heer, P. (2024). Experimental implementation of an emission-aware prosumer with online flexibility quantification and provision. *Sustainable Cities and Society*, 105531.Khayatian, F., Cai, H., Bojarski, A., Heer, P. and Bollinger, A., 2022. Benchmarking HVAC controller performance with a digital twin. *Applied Energy Symposium 2022: Clean Energy towards Carbon Neutrality (CEN2022)*.

Hekmat, N., Cai, H., Zufferey, T., Hug, G. and Heer, P., 2023, June. Data-driven demand-side flexibility quantification: Prediction and approximation of flexibility envelopes. In *2023 IEEE Belgrade PowerTech* (pp. 1-6). IEEE.

Yin, M., Cai, H., Gattiglio, A., Khayatian, F., Smith, R.S. and Heer, P., 2024. Data-driven predictive control for demand side management: Theoretical and experimental results. *Applied Energy*, *353*, p.122101.

Lédée, F., Padey, P., Goulouti, K., Lasvaux, S. and Beloin-Saint-Pierre, D., 2023. EcoDynElec: Open Python package to create historical profiles of environmental impacts from regional electricity mixes. *SoftwareX*, *23*, p.101485.

The following work-in-progress documents have been prepared using this report's scientific outputs partially documented.

Cai, H., Beloin-Saint-Pierre, D., Frossard, M., Bourdy, A., Lasvaux, S. and Heer, P. High temporal resolution short-term forecast of electricity carbon footprint for demand-side management. To be submitted.

Cai, H., et al. Spatiotemporal distribution of space heating demand flexibility potentials at national scale. To be submitted.

Cai, H., et al. Flexibility of commercial and residential energy hubs: simulation and experimental insights. To be submitted.

# 8 References


Armenise, G., Vaccari, M., Di Capaci, R.B., Pannocchia, G., 2018. An Open-Source System Identification Package for Multivariable Processes, in: 2018 UKACC 12th International Conference on Control (CONTROL). pp. 152–157. https://doi.org/10.1109/CONTROL.2018.8516791

Beloin-Saint-Pierre, D., Albers, A., Hélias, A., Tiruta-Barna, L., Fantke, P., Levasseur, A., Benetto, E., Benoist, A., Collet, P., 2020. Addressing temporal considerations in life cycle assessment. Science of The Total Environment 743, 140700. https://doi.org/10.1016/j.scitotenv.2020.140700

BFE, 2020. aramis project webpage "EcoDynBat – Ecobilan Dynamique des Bâtiments" [WWW Document]. URL https://www.aramis.admin.ch/Grunddaten/?ProjectID=41804 (accessed 1.23.24).

Bünning, F., Warrington, J., Heer, P., Smith, R.S., Lygeros, J., 2020. Machine learning and robust MPC for frequency regulation with heat pumps.

Cai, H., Heer, P., 2021. Experimental implementation of an emission-aware prosumer with online flexibility quantification and provision. arXiv preprint arXiv:2110.12831.

ecoinvent, 2020. ecoinvent Database. URL https://ecoinvent.org/the-ecoinvent-database/ (accessed 1.25.24).

Eggimann, S., Vulic, N., Rüdisüli, M., Mutschler, R., Orehounig, K., Sulzer, M., 2022. Spatiotemporal upscaling errors of building stock clustering for energy demand simulation. Energy and Buildings 258, 111844. https://doi.org/10.1016/j.enbuild.2022.111844

Electricity map, 2024. Live 24/7 $CO_2$ emissions of electricity consumption [WWW Document]. URL http://electricitymap.tmrow.co (accessed 1.25.24).

ENTSO-E, 2024. ENTSO-E Transparency Platform [WWW Document]. URL https://transparency.entsoe.eu/dashboard/show (accessed 1.25.24).

Fazel Khayatian, Hanmin Cai, Aaron Bojarski, Philipp Heer, Andrew Bollinger, 2022. Benchmarking HVAC controller performance with a digital twin. EnerarXiv.

Gasindustrie, gazenergie ch-V. der S., 2024. Mit Gas in die Energiezukunft [WWW Document]. URL https://gazenergie.ch/de/ (accessed 1.25.24).

Hekmat, N., Cai, H., Zufferey, T., Hug, G., Heer, P., 2023. Data-driven demand-side flexibility quantification: Prediction and approximation of flexibility envelopes, in: arXiv Preprint arXiv:2110.12796.

International Energy Agency, 2017. Digitalization and Energy.

Larimore, W.E., 1990. Canonical variate analysis in identification, filtering, and adaptive control, in: 29th IEEE Conference on Decision and Control. Presented at the 29th IEEE Conference on Decision and Control, pp. 596–604 vol.2. https://doi.org/10.1109/CDC.1990.203665

Lédée, F., Padey, P., Goulouti, K., Lasvaux, S., Beloin-Saint-Pierre, D., 2023. EcoDynElec: Open Python package to create historical profiles of environmental impacts from regional electricity mixes. SoftwareX 23, 101485. https://doi.org/10.1016/j.softx.2023.101485

Li, H., Wang, Z., Hong, T., Piette, M.A., 2021. Energy flexibility of residential buildings: A systematic review of characterization and quantification methods and applications. Advances in Applied Energy 3, 100054. https://doi.org/10.1016/j.adapen.2021.100054

Orehounig, K., Fierz, L., Allan, J., Eggimann, S., Vulic, N., Bojarski, A., 2022. CESAR-P: A dynamic urban building energy simulationtool. JOSS 7, 4261. https://doi.org/10.21105/joss.04261

Roux, C., Schalbart, P., Peuportier, B., 2017. Development of an electricity system model allowing dynamic and marginal approaches in LCA—tested in the French context of space heating in buildings. Int J Life Cycle Assess 22, 1177–1190. https://doi.org/10.1007/s11367-016-1229-z

SFOE, 2020. aliunid - Versorgung «neu»: Feldtest 1.1.2019 – 30.6.2020 - Basic data [WWW Document]. URL https://www.aramis.admin.ch/Grunddaten/?ProjectID=43459 (accessed 1.25.24).

Van Overschee, P., De Moor, B., 1994. N4SID: Subspace algorithms for the identification of combined deterministic-stochastic systems. Automatica, Special issue on statistical signal processing and control 30, 75–93. https://doi.org/10.1016/0005-1098(94)90230-5

VERHAEGEN, M., DEWILDE, P., 1992. Subspace model identification Part 1. The output-error state-space model identification class of algorithms. International Journal of Control 56, 1187–1210. https://doi.org/10.1080/00207179208934363

Vuarnoz, D., Jusselme, T., 2018. Temporal variations in the primary energy use and greenhouse gas emissions of electricity provided by the Swiss grid. Energy 161, 573–582. https://doi.org/10.1016/j.energy.2018.07.087

Yin, M., Cai, H., Gattiglio, A., Khayatian, F., Smith, R.S., Heer, P., 2024. Data-driven predictive control for demand side management: Theoretical and experimental results. Applied Energy 353, 122101. https://doi.org/10.1016/j.apenergy.2023.122101

# 9 Appendix

## 9.1 Procedure to calculate the GHG content of the Swiss hourly mix

### 9.1.1 ENTSO-E Files for raw data on electricity production and exchanges

First, we need the input data from the ENTSO-E Platform. Download the files via Filezilla as follows:

1 Install FileZilla on your computer
2 Create an account on https://transparency.entsoe.eu
3 In FileZilla:
  3.a Host: sftp://sftp-transparency.entsoe.eu
  3.b Username: address of ENTSO-E account
  3.c PW: same as for ENTSO-E account
  3.d Port: 22
4 Navigate the files with the data available
  4.a Download files from folder: CrossBorderPhysicalFlow
  4.b Download files from folder: AggregatedGenerationPerType

The ENTSO-E platform provides many data on electricity. We use the datasets on exchanges between countries and national energy generation by energy sources for CH countries and neighboring countries at different time steps (i.e., 15 minutes and hourly). This step is now down automatically carried out every hour with an extraction algorithm in Python.

### 9.1.2 LOSSES (file: pertes_OFEN in SUPPORT_FILES)

Fill, by hand, the data files (Excel or CSV) that inform the algorithm on the Swiss Electricity Statistics (PDF files for each year). For all the columns of the Losses file, the values are entered. This information will be updated every year when BFE releases new information.
The PDF documents for the Swiss Electricity Statistics can be found:
https://www.bfe.admin.ch/bfe/en/home/supply/statistics-and-geodata/energy-statistics/electricity-statistics.html

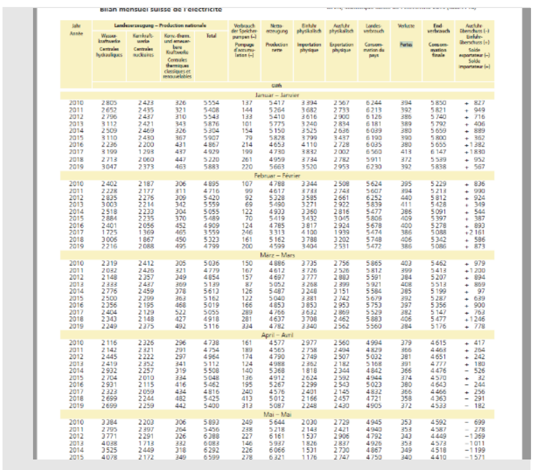

### 9.1.3 RESIDUE (file: Repartition_Residus in Support_Files)- means of electricity production

Fill, by hand, the data files (Excel or CSV) that inform the algorithm on the SFOE publication for Swiss Electricity Statistics (PDF files for each year). These files are located: https://www.bfe.admin.ch/bfe/en/home/supply/statistics-and-geodata/energy-statistics/electricity-statistics.html

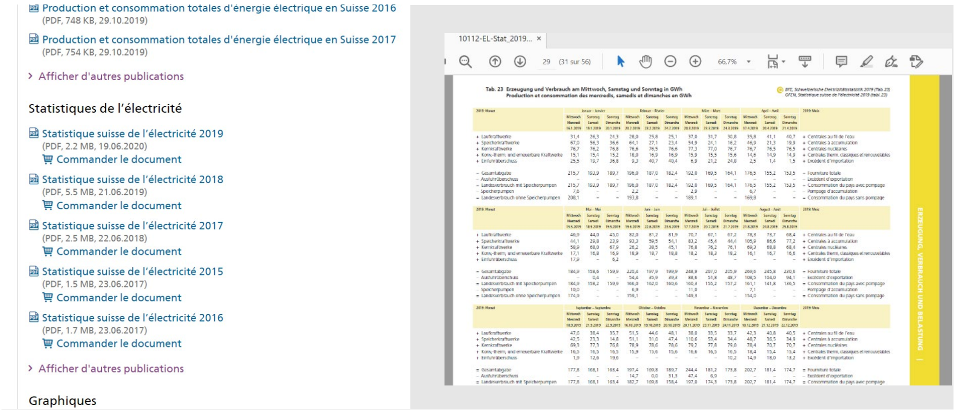


### 9.1.4 ENTSO-E data for the same days as the "standard days" of the SFOE publication

Next, you have to search the ENTSO-E data for the same days and fill in the Repartition_Residus.xlsx file. All other rows are formulas calculated automatically based on the data from steps 4 and 5. This can be done with the FTP site of the ENTSO-E platform (see sec. 1)

### 9.1.5 Swissgrid (file: swissgrid_total in Support_files) total elec consumption and production

Fill in values (by hand). The file can be found: https://www.swissgrid.ch/en/home/operation/grid-data/generation.html

In the consumption and production chapter of network data, by Statistics, at the end of the page:

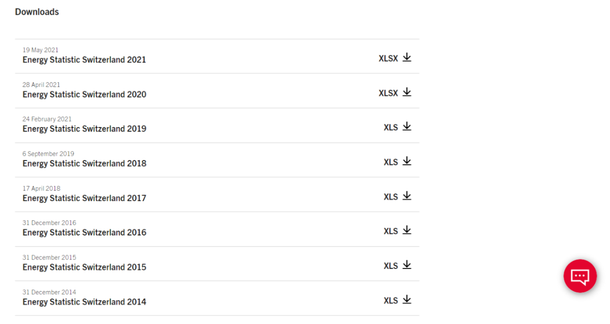


### 9.1.6 Finally, run the Python code: 20211126_EcoDB_execute.py

This algorithm automatically:

- extract the ENTSO-E data every hour when the platform is updated
- transform the ENTSO-E raw data into a usable CSV file
- Use all the mentioned data sources to create a 15-minute CF profile for the Swiss electricity mix with up-to-date information that can be used to forecast the CF of the next 24-48 hours.

## 9.2 Single-line diagrams of the infrastructure and upgrade

| | Empa move / NEST / ehub | K3 Handwerkcity |
|---|---|---|
| | 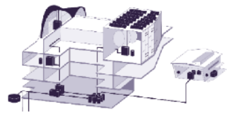 |  |
| m² | 4'500m2 Wohnungen und Büros | 7'100m2 Geschäfte und Büros |
| | In Betrieb seit 05.2016 | In Betrieb seit 06.2020 |
| | Empa Verteilnetz | *die werke* Verteilnetz |
| | 10'000 Datenpunkte alle 1min | 2'000 Datenpunkte alle 15min |
| | 122kWp | 669kWp |
| | 169kWh | / |
| | 142kW$_{th}$ – ground source | 280kW$_{th}$ – air source |
| CH₄ | / | 61kW$_{th}$ |
| | 7'700lt. | 11'900lt. |
| | 4 EV-Ladestationen | 4 - 80 EV-Ladestationen |
| www | https://www.empa.ch/web/energy-hub/ | https://www.diewerke.ch/handwerkcity |

Figure 54. Summary of infrastructure at K3 and NEST.

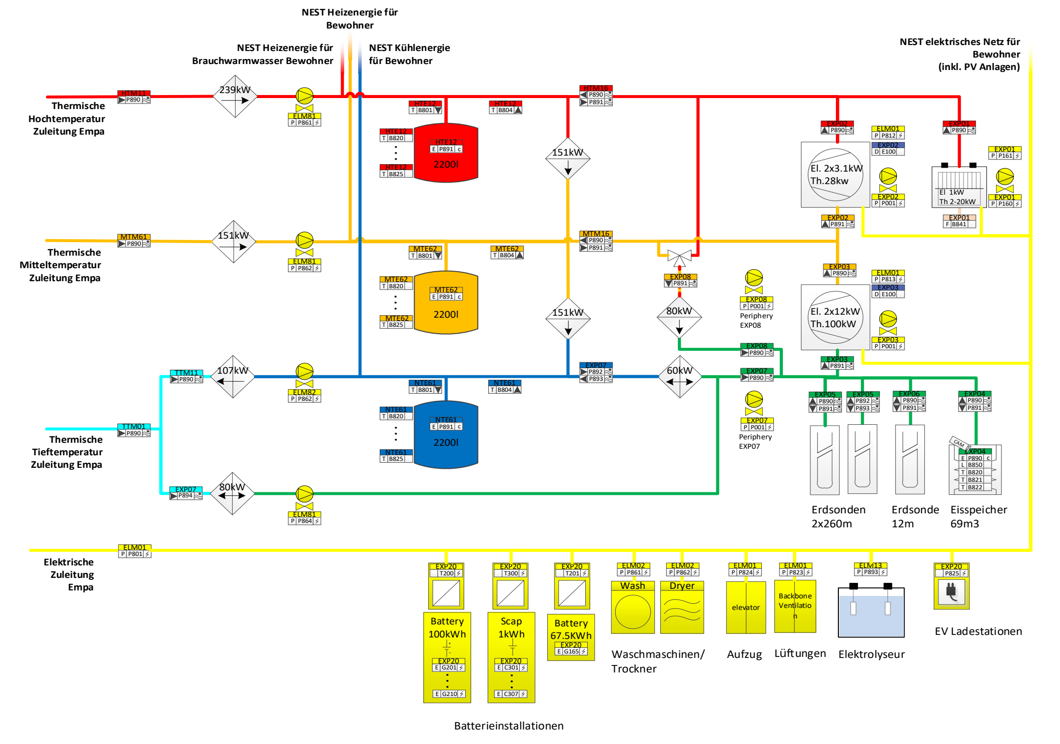


Figure 55. Single-line schematic of the energy hub at NEST.

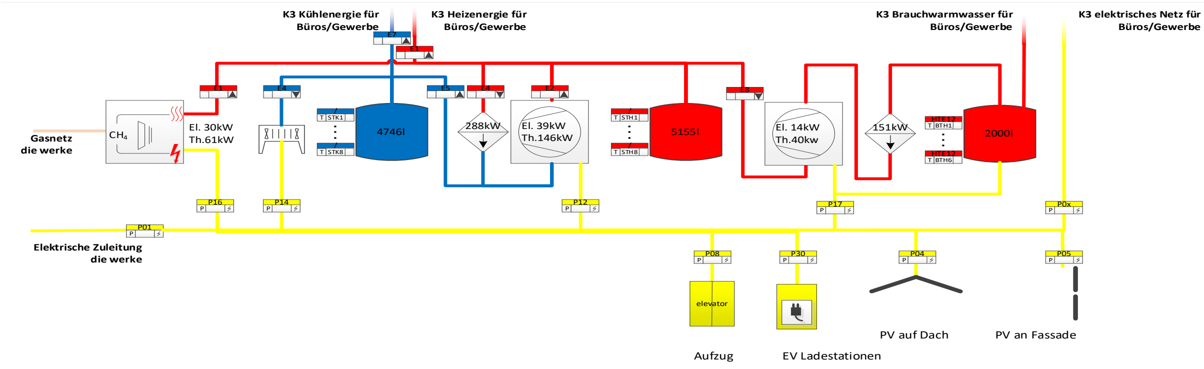


Figure 56. Single-line schematic of the energy hub at K3.

The implementation of the interface between the EMS and K3 suffered a delay of four months and is expected to be ready by the end of January 2022.
The current implementation is a closed system with a daily data export to an FTP server, as seen in blue in Figure 57. To control the system via an EMS, data needs to be read from the system in with an update rate of 5 min and data needs to be sent to the infrastructure, to impact the systems behavior. As for reading data, there is an interface envisioned via an API provided by Invisia. 99 signals were identified to be relevant for real-time observability of the system.

As for sending data, an existing interface between the components (HPs, CHP) and the local Invisia data collection shall be extended; then, the same API as for reading real-time data can be used to send data to the infrastructure. 17 Datapoints (i.e., 15 Setpoints and 2 watchdog signals) are foreseen to be sent every 5 minutes.

We have defined a comprehensive list of data points needed to implement the EMS. I.e., a predictive controller that retrieves data periodically and sends set points based on optimization results.

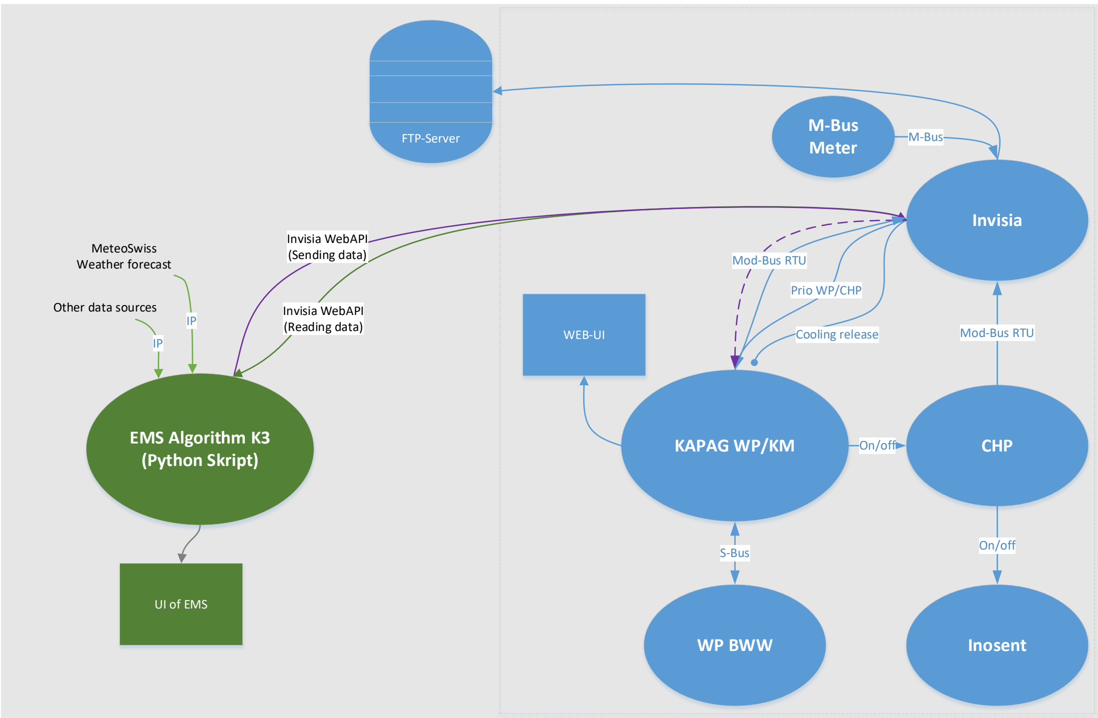

Figure 57. Communication interfaces between existing infrastructure (blue) and new EMS (green and purple). Sending data (purple) requires adaptions in current implementation on Invisias' and KAPAGs side.